CHALMERS
UNIVERSITY OF TECHNOLOGY

Chalmers University of Technology

Automotive Engineering Project

Aerodynamic investigations of a bus under high side wind conditions

Authors:
Oskar Hellsten
Oskar Pettersson
Matus Minar
Hugo Gefors
Birk Forsström
Nithin Bharadwaj Ravindra

Examiners:
Jonas Sjöblom
Supervisors:
Simone Sebben
Alexey Vdovin

January 30, 2020

Abstract

The Norwegian Public Roads Administration (NPRA) is looking for different solutions on how to shorten the travel time for road vehicles between Bergen and Trondheim. The main reason for the long traveling time is due to the amount of fjords that needs to be crossed by ferries when traveling by the coast. Because of this several alternatives to ferries are explored and one of these alternatives is using floating bridges. Since side winds affect the stability of the floating bridge coverage of the sides will be minimal and therefore all vehicles will be fully exposed to side winds. Larger vehicles like buses and trucks are the main concern in regards to sudden instability or a rollover. To prevent accidents it has been decided that a vehicle dynamic model will be made to evaluate the wind speed threshold for when the bridge should be closed or the vehicle speed should be limited. The magnitude of the side forces on long vehicles during high wind conditions is needed as an input to create this vehicle dynamic model. By using CFD together with wind tunnel testing with a scale model an investigation of these forces has been performed.

A scale model of the Volvo 9700 series coach bus was 3D printed to be used for wind tunnel testing. Because of a predetermined available mounting area as well as with regards to wind tunnel blockage ratio a scale of 1:18 was chosen. The model was then printed in 9 different parts excluding the wheels because of print volume limitations. To be able to try different design configurations the model was made modular. The front and rear were attached using neodymium magnets while the other parts were either permanently attached using epoxy based glue or screws together with threaded inserts that were melted in to fuse with the plastic. To get a good surface finish for added accuracy in the wind tunnel the model was covered with body filler, sanded, then covered in spray filler and lastly painted black.

The wind tunnel testing of yaw angles covered a complete 360° sweep with increments of 5° up to 90° and then increments of 10° for the rest. The results were mainly used as reference to the CFD results since the wind tunnel setup did not include rotating wheels and boundary layer suction. Visualization of the airflow around the bus was achieved by using tufts, smoke and thermal camera.

A steady state incompressible RANS equations(Reynolds Averaged Navier Stokes) are numerically solved in StarCCM+ to determine forces and moments. These forces were determined by running simulations for a changing yaw angle from 0 to 90° in 5° steps. Non-dimensional co-efficients of drag force, lift force, side force, yaw moment, roll moment and pitch moment are calculated to compare the data from wind tunnel. This is done as the wind tunnel testing is obtained for a scaled model and in CFD the actual size of the bus is used. Results show that the trends observed in CFD follow the trends from wind tunnel test data.

It was observed that coefficient of side force and roll moment increases with the increasing yaw angle and reaches a maximum value at 90° yaw. This shows the importance of the effect of cross winds on vehicles with large side area. This data can be further used in a vehicle dynamic model to evaluate the impact on vehicle stability.

Contents

List of Figures

1 Introduction

1.1 Background

The Norwegian Public Roads Administration (NPRA) is looking for different solutions on how to shorten the travel time for road vehicles between Bergen and Trondheim. Today the road along the coast includes ferries to cross the fjords, which is time consuming. Different alternatives to the ferries are investigated and one of those is a floating bridge. Since a floating bridge is sensitive to high wind the bridge is built to minimize the surface area that is exposed to the wind. This leads to that the vehicles that travel on the bridge are less protected from side winds.

Vehicles that have a large side area are more exposed to side wind forces and more sensitive to roll over and lateral instability compared to a passenger vehicle. Due to that heavy side winds could occur the NPRA wants to be able to give recommendations on when vehicles with large surface area should reduce the speed over the bridge or even if the bridge should be closed for these vehicles if the conditions are too harsh. In order to be able to make that recommendation the resulting forces from side winds should be investigated. The vehicle that is to be investigated is a generic bus model that is based on a Volvo 9700 coach bus, as it is one of the target vehicles for this project due to the large side surface area. The results from this project will contribute to a larger research project about the floating bridges.

1.2 Goal Statement

The goal of the project is to:

- Simulate heavy side wind conditions on a bus.
- Build a scale model of the simulated bus for wind tunnel testing.
- Run actual tests in the wind tunnel.
- Make the bus scale model modular with interchangeable parts for future use in Chalmers courses.
- Obtain data on forces and moments that act on the bus, to serve as input in future research.

2 Literature Study

To understand and analyze the effects of side winds on vehicles a literature study of previous work in the area was performed, regarding the effects of cross wind on buses and trucks. A study on crosswind aerodynamics for road vehicles [1] by Youhanna E. William et al addresses a method aimed at developing a 3D Computational Fluid Dynamics (CFD) model for an actual bus to predict the impact of the crosswind on the overall aerodynamics. The study found that there are higher lift and side forces acting on the bus under higher angled cross wind, when compared to the drag forces.

A study made on a heavy truck passing a bridge pylon [2] by Salati L. et al investigated the aerodynamics forces acting on heavy goods vehicle (HGV) during the overtaking on a bridge tower when the vehicle is passing through the wake generated by lateral wind. A dynamic or moving mesh technique was used in the simulate the relative velocity between the vehicle and infrastructure. They found that there is transient pressure distribution on the surface of HGV from cabin to trailer while passing through the bridge pylon which has an effect on side forces and yawing moment on the bus.

Xiang H. et al made a study on moving vehicles under crosswind [3] in which the vehicle is made to move along a guide way that can adjust to wind directions to see the effect of five-component coefficients over crosswinds. It was found that the five coefficients had a similar trends of variation in yaw as compared to zero yaw but the side force and yaw moment coefficients were smaller compared to zero yaw.

In a study on unsteady aerodynamic responses to wind [4] by Yamashita T. et al a wind tunnel nozzle was developed with oscillating plates and airfoils for a full-scale wind tunnel to simulate the natural wind which induces more unsteady aerodynamics forces when compared to normal wind tunnel case. The oscillating plates produced a transient wind velocity fluctuation and airfoils provided fluctuations of yaw angle. A full-scale hatchback vehicle model was used in the wind tunnel with the developed nozzle to observe that the unsteady aerodynamic forces are larger than the steady aerodynamic forces. They also found that the unsteady aerodynamic response characteristics are controllable to a great extent by modifying external contour of vehicle.

These studies emphasise the importance of the side wind forces on the stability of the vehicle. However most of the studies found were on trucks and for yaw angles less than 30°. The current study focuses on the effect of wind at yaw angles up to 90° to provide information on the effect of side wind on buses moving over a bridge.

3 Virtual Model

Based on a Volvo 9700 model received from Volvo Bus a Computer Aided Design (CAD) model was created in the commercial CAD software Catia V5 2019. Simplifications to the bus body geometry were made to get a model with enough detail to simulate the actual bus but without details that will be to small to be seen in the later printing stage. The rims of the bus were modeled as flat and solid, both in order to simulate the deflection and contribution of the wheel and also make the CFD meshing easier. As for the underside of the bus it was made flat since the model received from Volvo Bus had a flat floor. At 0 yaw the frontal area of the bus is 8.5 m^2. The CAD model created can be seen in figure 3.1.

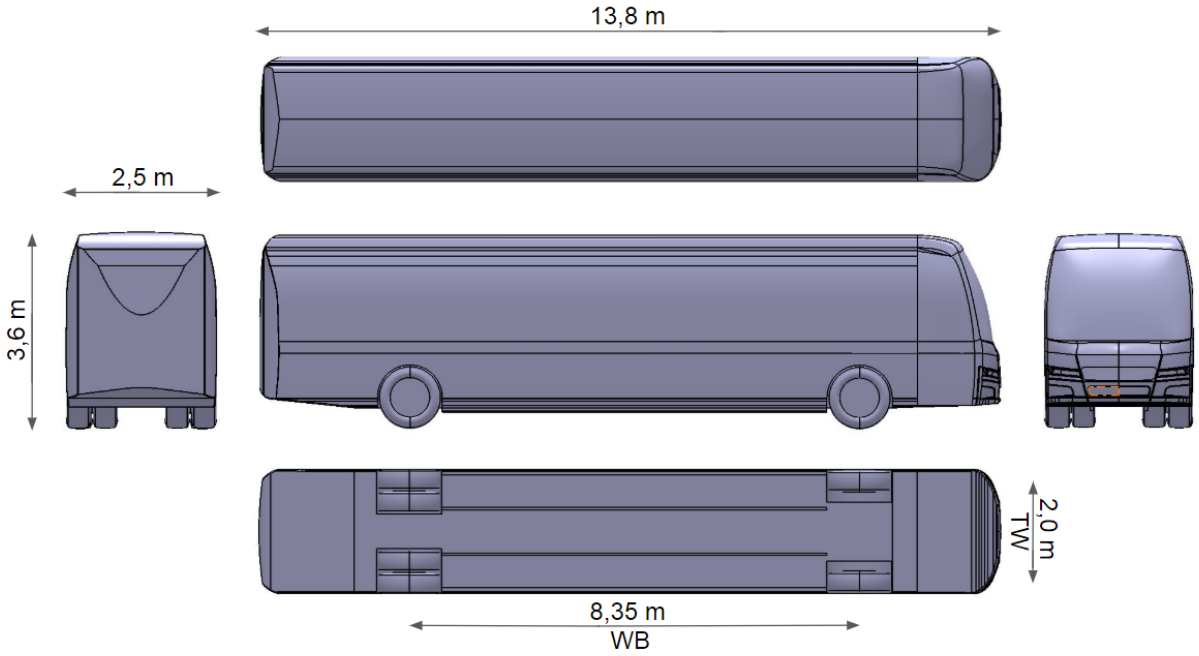

Figure 3.1: Picture of the bus used in CFD and wind tunnel created in Catia

4 CFD Model

The CFD analysis begun with setting up a model of the full scale bus, using StarCCM+ 13.06.11. The needed geometry of the bus was imported from a 3D CAD from the Catia model, subsequently, the model was meshed, analyzed and post processed in StarCCM+.

The forces in three directions are referred to as drag, side and lift forces in x, y and z directions respectively. Moments, which result from these forces are regarded as roll, pitch and yaw moment in x, y and z directions respectively. The origin of the coordinate system to measure these moments was based into the center of the wheelbase, track width and at the ground in z direction as shown in figure 4.1.

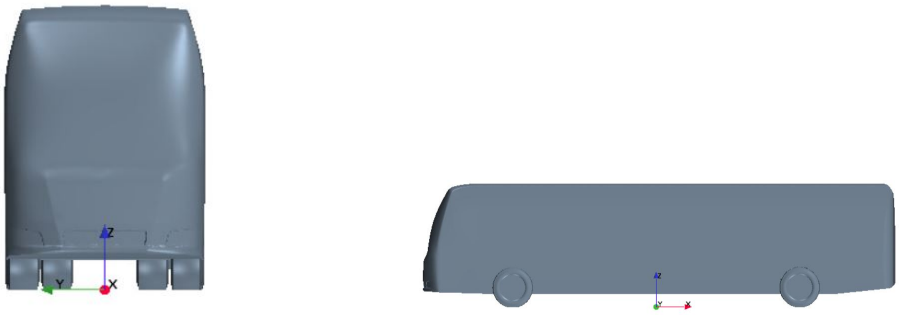

(a) Front View (b) Side View

Figure 4.1: Axis about which moments are calculated

The coefficient of forces and moments in x, y and z directions are given by equations 4.1 to 4.6.

$$Cd = \frac{2 * F_x}{\rho * v^2 * A} \tag{4.1}$$

$$Cs = \frac{2 * F_y}{\rho * v^2 * A} \tag{4.2}$$

$$Cl = \frac{2 * F_z}{\rho * v^2 * A} \tag{4.3}$$

$$Cmx = \frac{2 * M_x}{\rho * v^2 * A * L} \tag{4.4}$$

$$Cmy = \frac{2 * M_y}{\rho * v^2 * A * L} \tag{4.5}$$

$$Cmz = \frac{2 * M_z}{\rho * v^2 * A * L} \tag{4.6}$$

Where F_x, F_y and F_z are forces in x, y and z directions respectively, M_x, M_y and M_z are moments about x, y and z axis, ρ is the density, v is the velocity at 0° yaw angle case, A is the frontal area and L is the wheelbase of the bus [3]. These non-dimensional coefficients are calculated so that they can be compared with wind tunnel results which are done on a scaled model. The reference frontal area, velocity and wheelbase remained the same for all the angles which makes it possible to compare forces and moments at different yaw angles.

4.1 Computational Domain

The computational domain was chosen in a way, that the yaw angle sweep study could be performed without changing the volume mesh for each angle. It's size was based upon the literature studies done in the beginning of the project. The aim was to make it big enough, so that the influence of the boundary conditions on the results would be minimized. Furthermore, the dimensions of the wind tunnel were adjusted to dimensions mentioned in study made by William Y.E. et al [1], 15 times the length of the bus in length, 38 times the width of the bus in with and 12 times the height of the bus in height.

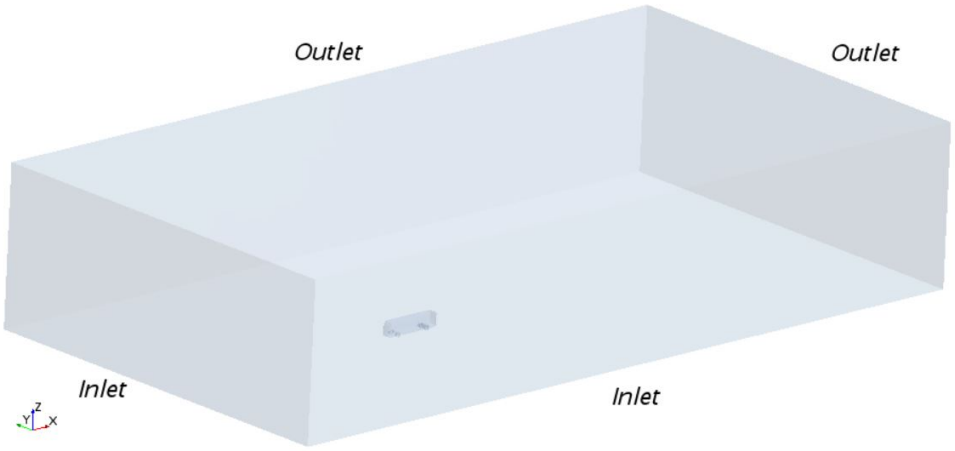

Figure 4.2: Computational domain

4.2 Mesh

The construction of mesh was executed using polyhedral mesher, surface mesher and prism layer mesher tools. Polyhedral cell mesher tool was chosen due to its ability to provide efficient mesh with minimal skewed cells even for complex geometries. On top of that, according to recommendations[11], in simulations involving free stream variation in angles, the polyhedral mesh performs better than trimmed, due to it's pseudo-random orientation of faces. As a result of the complexity of the model and limited amount of the computational resources, the volume of the domain was divided into refinement zones with a specific cell size for each of them using the volumetric refinements. Naturally, the closest refinement zone to the bus model contained the smallest cells, subsequently, their size progressively grew in each cube closer to computational domain boundaries. The idea of the prism surface layer was to capture the flow shear stresses in the boundary layer, therefore it was only used on the bus surface.

The mesh refinement was continuously adjusted until the correct value of wall y^+ for the corresponding turbulence model was obtained. In addition to that, in order to secure convergence and capture all key flow physics a proper transition in cell sizes between adjacent mesh volumes was

required on top of good overall quality of the mesh with a minimum skewed cells. As mentioned before, the computational resources were limited and this required a careful strategy to run more simulations without compromising the accuracy of the results.
Wall y^+ value depends on the thickness of the first cell near the wall where the boundary layer begins. y^+ at a distance is defined as in equation 4.7,

$$y^+ = \frac{u_\tau * y_N}{\nu} \tag{4.7}$$

where u_τ is the friction velocity, y_N is the thickness of the first cell and ν is the kinematic viscosity.

Due to the fact that it is not possible to find the exact value of the wall $y+$ before solving the fluid flow, an initial guess was required. It was determined using a correlation for skin friction on thin flat plate with undeveloped flow approaching the leading edge of the flat plate.[5] This correlation is used to calculate the friction velocity u_τ. Equation 4.7 can be re-written as in equation 4.8,

$$y_N = \frac{y^+ * \nu}{\sqrt{0.0592 * Re^{\frac{-1}{5}} * (\frac{{U_\infty}^2}{2})}} \tag{4.8}$$

where Re is the Reynolds number and U_∞ is the free stream velocity. Reynolds number is calculated for a thin plate of length equal to the length of the bus. Using the computed Reynolds number, the desired y^+ value for an initial guess could be made.

The desired y^+ value depends on the turbulence model and y^+ wall treatment models of the selected turbulence model. The study made by William Y.E. et al [1] showed that the realizable $k-\epsilon$ turbulence model was most accurate when compared to the experimental measurements. Hence this turbulence model was used to solve the problem at hand.

All y^+ wall treatment is selected in our model as it is designed to give similar results to low-y^+ treatment for $y^+ \leq 1$ and to high-y^+ treatment for $y^+ > 30$. It was decided to keep the wall y^+ between 30 - 100 with few cells having y^+ below 30 which is acceptable according to recommendations on Steve portal[7].

Using equation 4.8 an initial guess is made:

$y^+ = 30$:
First cell thickness = 0.001 m
No. of layers = 3
Total thickness of prism layer = 0.00225 m

These values were later on modified in the model based on the results obtained from these initial settings. The final mesh contains 58 million cells. Figure 4.3 displays the final mesh around the bus, in the wake side for yaw and near the wall.

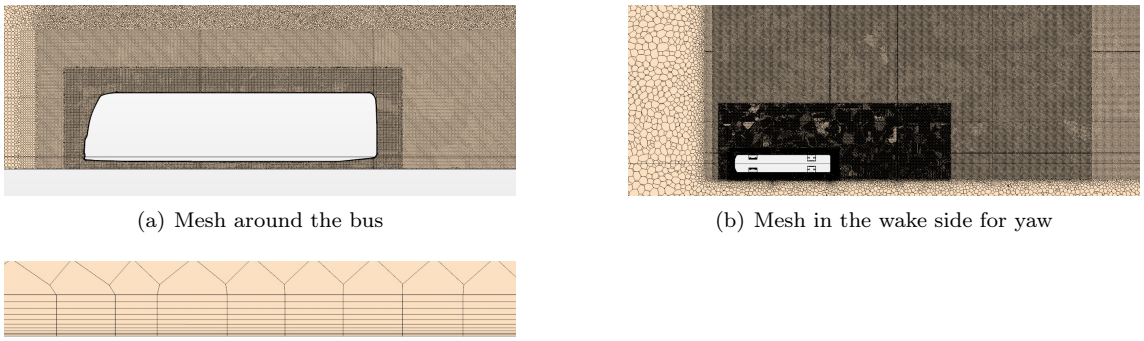

(a) Mesh around the bus

(b) Mesh in the wake side for yaw

(c) Mesh closer to the wall

Figure 4.3: Mesh scene

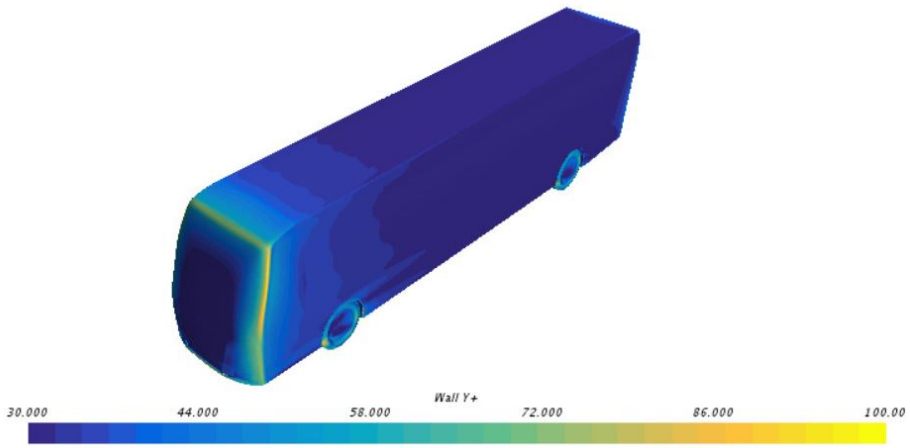

Figure 4.4: Wall y^+ for reliazable $k - \epsilon$ model

4.3 Physics and Boundary Conditions

A steady-state incompressible RANS equation is numerically solved in StarCCM+ using a coupled flow solver. The settings for this solver are chosen based on best practice recommendations [8]. In addition to this, grid sequencing initialization is used which utilises the solution from a coarse mesh to initialise before solving the problem. This initialization helps the solution to converge faster for realizable $k - \epsilon$.

Boundary conditions specified, as shown in figures 4.2 and 4.5, are

- Inlet - Velocity Inlet : (v*$cos\alpha$, v*$sin\alpha$, 0)m/s
- Outlet - Dirichlet condition for Pressure Outlet
- Ground - Moving ground with $v = 27.78m/s$ in the direction opposite to the motion of the bus, no slip condition

- Symmetry - A Symmetry condition is defined on the top boundary of the domain.
- Bus - Standard Wall, no slip condition
- Wheels of the Bus - Rotating wheels with tangential velocity that is equal to the velocity of the moving ground.

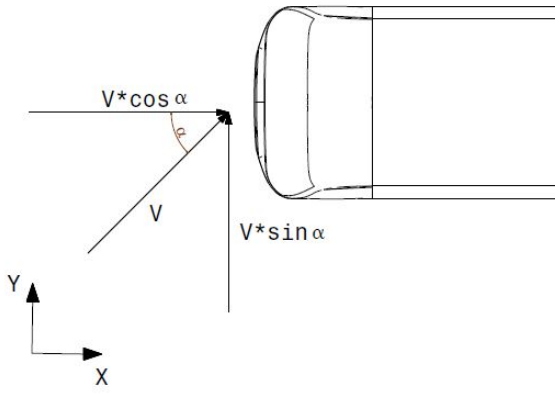

Figure 4.5: Velocity vectors

As shown in figure 4.5 the cross wind with velocity v, is split into vertical and lateral components. Angle α is the yaw angle which is varied from 0° to maximum of 90°. The value of v is fixed and does not change when the yaw angle sweep is made. The value of v for CFD is taken as maximum velocity of a typical bus, i.e. $27.78m/s$ ($100km/h$).

4.4 Convergence Criterion

To judge the convergence, a specific criteria had to be simultaneously taken into account. The first requirement was to obtain the momentum, energy and continuity residuals that should drop by more than three orders of magnitude. Secondly, the coefficient of drag should not change by more than one count for 500 iterations. In case of this project, one count is equal to 0.001. Figures 4.6 and 4.7 shows residuals and Cd values for a converged solution of zero yaw.

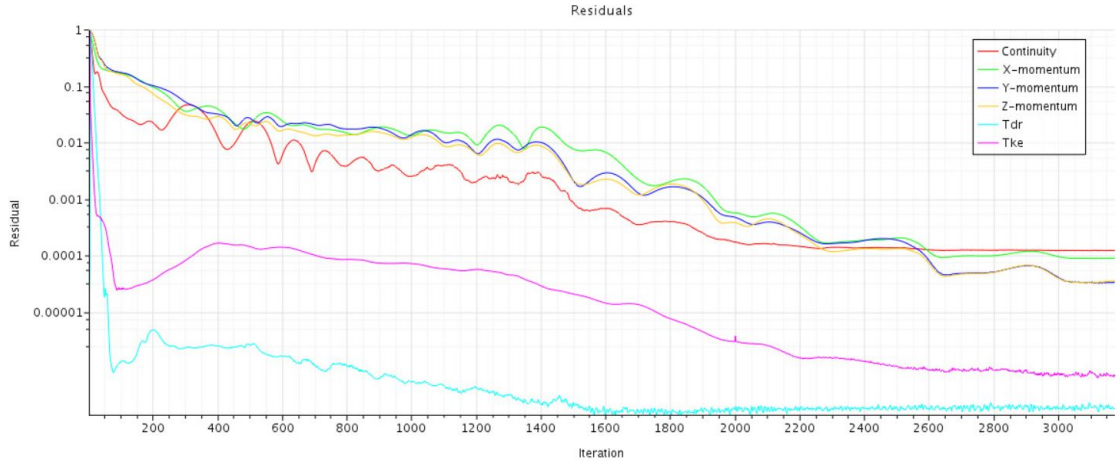

Figure 4.6: Residuals

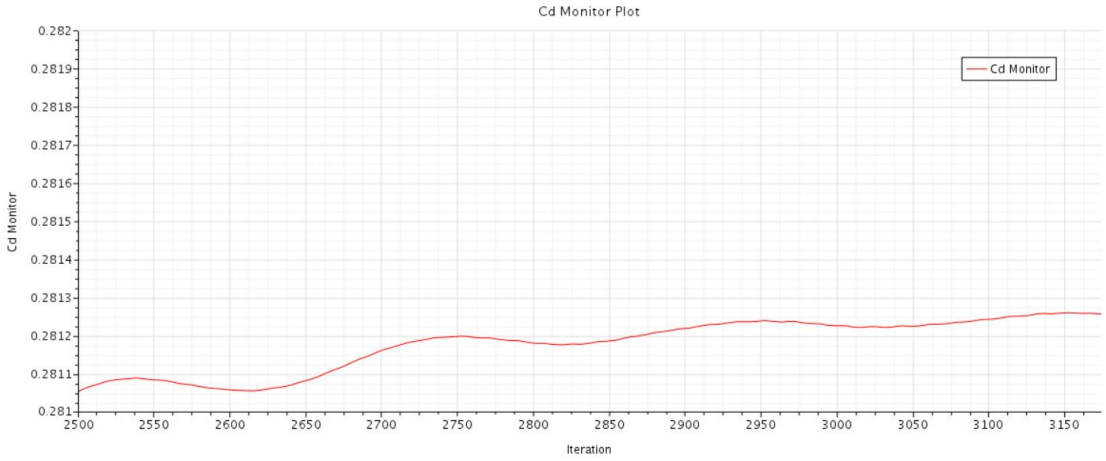

Figure 4.7: Drag coefficient

4.5 Mesh Independence Study

The main purpose of performing a mesh independence study, is to prove that the increasing or decreasing level of resolution does not have a major impact on the results. In case of this specific project, several different mesh setups were tested, with a benchmark of 58 million cells. In figure 4.8 the plot displays the variation in value of Cd with either decrease or increase in number of cells, it's final value should be stabilized for 3rd decimal place - for one count. Based upon this plot, it was decided to continue with 58 million cells, since the deviation from other Cd values was not substantial. In addition to that, running simulations with more cells would be computationally costly, therefore the chosen value of cells was based on this criterion as well.

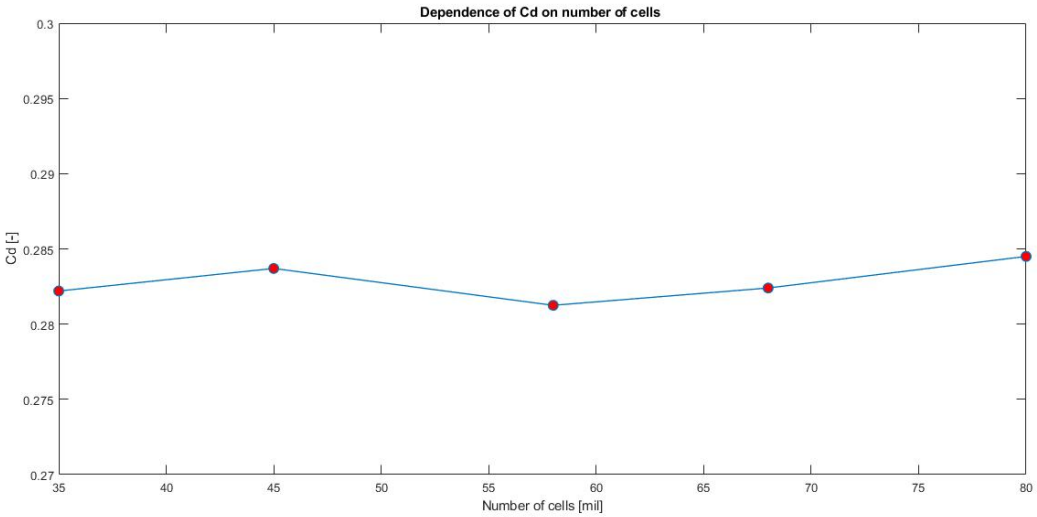

Figure 4.8: Dependence of Cd on number of cells

5 Wind Tunnel

To validate the result and trends from the CFD simulation the same tests were done in a wind tunnel. The process started off with building a scaled model of the bus and a device to mount it on a scale in the wind tunnel and ended with analysing the collected data.

5.1 Bus Scale Model

In this section the process of how the size of the scale model were decided is explained. There is also a step by step description of how the model is manufactured from 3D printer filament to a finished bus model.

5.1.1 Scaling of the Model

First of all the size of the scale model had to be decided, the primary limiting factor was the size of the test section in the wind tunnel at Chalmers. To minimize blockage in the tunnel the model should be small, but the smaller the model is the higher the required wind speed needed is to achieve the same Reynolds number as with a full scale model. Blockage effect is the compression of air between the test object and the walls of the wind tunnel. The second limiting factor was the measurement restrictions of the scale used in the wind tunnel in regards to the maximum readable moments and forces of the scale, which is $60Nm$ and $300N$. The third limiting factor is the ground plate used in the tests that limits the length of the bus. As a result of this, the wheels needs to fit within a certain area, this will be further explained in the mounting plate section.

Based on these three limiting factors it was calculated that a scale model with a size of 1:18 would fulfill all the requirements. This size of scale 1:18 is the largest that can fit through the hole in the ground plate of the wind tunnel and the size is also small enough so that blockage will not be an issue and maximum tolerated forces of the scale will not be reached. Maximum forces on the scale were calculated with four inputs, Cd, wind speed, length of moment arm and projected area with equation 5.1 and 5.2. For Cd a value of 1.05 for a box were used, wind speed v was the maximum of $60m/s$ of the wind tunnel, moment arm of $l = 0.2$ m was twice as long as needed and projected area was the side area of the bus, $0.135m^2$. This resulted in maximum values of just over the limits but in the tests the wind speed will be around half and Cd will be lower so therefore it is assessed as acceptable.

$$F = \frac{1}{2} \cdot 1.25 \cdot Cd \cdot A \cdot v^2 = 318N \tag{5.1}$$

$$M = F \cdot l = 63Nm \tag{5.2}$$

5.1.2 Dividing the Model for 3D Printing

To be able to print the bus in the available 3D printers, which has a limited build area, at Chalmers the bus had to be divided into pieces. In figure 5.1 it's possible to see how the bus is divided into the different modules. The upper and lower center part had to be divided into three parts to be able to fit into the building area of the printer.

To make the model modular it was divided in a way which makes it possible to change from one to two rear axles and have interchangeable front and rear parts of the bus. This was done to be able to test different combinations of shapes and see the impact of the design. The three different fronts created were a normal bus front, an American school bus and a front of a high speed train. For the back end of the bus a more aerodynamic roof drop rear was designed along with the normal rear part. All available configurations of front and rear parts can be seen in figure 5.1.

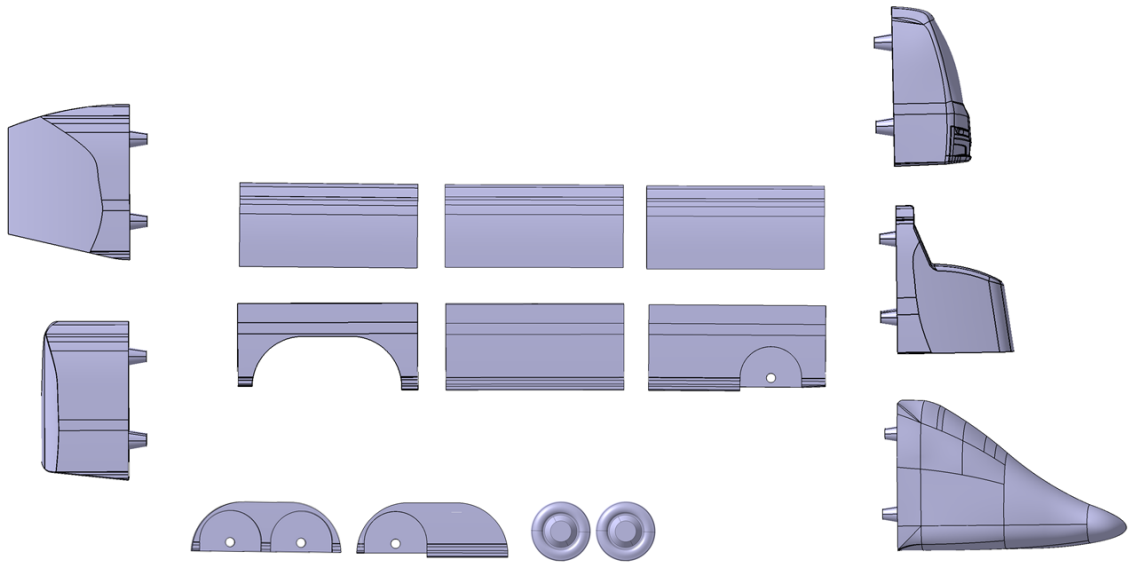

Figure 5.1: Exploded view of the bus model parts

5.1.3 3D Printing

Polylactic Acid (PLA) is a suitable plastic for 3D printing due to it's ability to stick to the build plate just enough that it does not detach during operation whilst it is still easy to remove when the part is completed. Another big concern when using fused deposition modeling (FDM) 3D printing is layer to layer adhesion and material shrinkage [10]. These problems can, when occurring together, create gaps in the model where the layers has detached and the material between the detached layers has shrunk as seen in figure 5.2. PLA has both good layer to layer adhesion as well as low shrinkage in comparison to other thermoplastics with similar melting point which therefore is suitable for FDM 3D printing. This is especially important when printing big parts that is larger than a cube measuring $10cm$ per side. There are downsides to PLA that has to be dealt with, the most concerning one is that it is a very brittle material making it unsuitable for threading. By using threaded inserts that are fused to the part by melting them into the plastic a good joint can be achieved despite the mechanical properties of PLA.

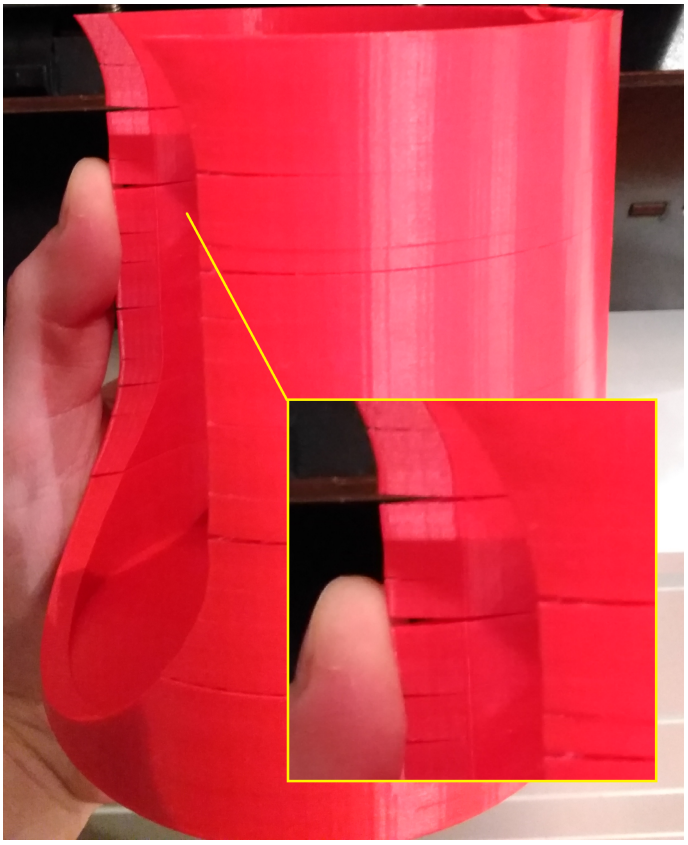

Figure 5.2: 3D printed part with layer to layer separation due to material shrinkage. The material used is acrylonitrile butadiene styrene (ABS)

3D printing usually requires a lot of testing to achieve good quality, both regarding strength and surface quality. The reason has a lot to do with material differences, once the software parameters are correctly set up for a specific brand and type of material the main problems associated with 3D printing is dealt with. Unfortunately all PLA materials are not comparable due to additives used by the manufacturers to make the material have specific properties.

The 3D printer used for printing all the parts for the bus model was a Prusa MK3S [12]. The MK3S has a print plate with a surface covered in a plastic called polyetherimide (PEI) which has good properties regarding adhesion to a lot of plastic printing materials including PLA. Although a lot of surface treatments or coatings can be used for adding adhesion as well as easier detachment for print materials PEI is one of the most versatile choices and compared to temporary treatments, like glue stick or hair spray which often is used in 3D printing, it offers the least amount of preparation and clean up.

The bus model is made using PLA from the manufacturer Add:north. It was evident during the first test prints that the material has tendencies to shrink when the surrounding air temperature is at normal room temperature. This lead to the bottom layer detaching from the build plate in the corners during printing. The preferable solution to avoid this would be to have a temperature controlled volume around the printer but since the printer that was used is a lent piece of equipment it was not possible to modify or alter the machine in any way. An alternative compromised solution to the problem is to add something called a brim to the parts. A brim is a added area for increased adhesion to the build plate that only concerns the first layer of the printed part.

Printing parameters regarding wall thickness, which concerns the amount of layers used for the perimeters, and infill density was chosen mainly to accommodate the mounting of threaded inserts.

Since the inserts required a minimum wall thickness of 3.3 mm which also makes the part very strong the infill could be really sparsely and was therefore set to 5% [9]. An example of a completed 3D print can look as in figure 5.3.

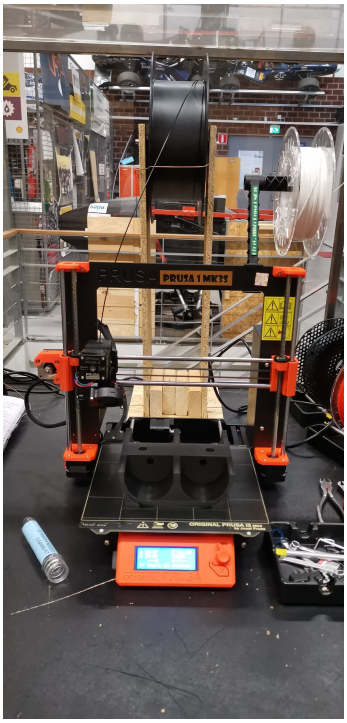

Figure 5.3: The Prusa MK3S 3D printer with a finished part of the bus on the build plate

5.1.4 Model Assembly

When all the parts had been printed the model could be assembled through various means. The three roof parts and the corresponding three floor parts were glued together separately and then screwed together. To be able to screw the roof and floor together M6 screw inserts have been melted into the roof part. Holes in the bottom of the bus allowed access for the screws to the inserts. The same M6 screw inserts were melted into the bottom part that holds the rear axle inserts, in this way the rear axle part can be interchanged.

The front and rear ends of the bus were to be attached to the bus body using neodymium magnets attached to the end of the three alignment pins present on each of the front and rear parts. To make the wheel axles more robust so that they do not break apart they were made from steel instead of PLA plastic. The wheel axles were glued into the axle holes in the body and the wheels were then glued onto the axles. In figure 5.4 and 5.5 it is possible to see detail pictures of the both the screw inserts and the neodymium magnets.

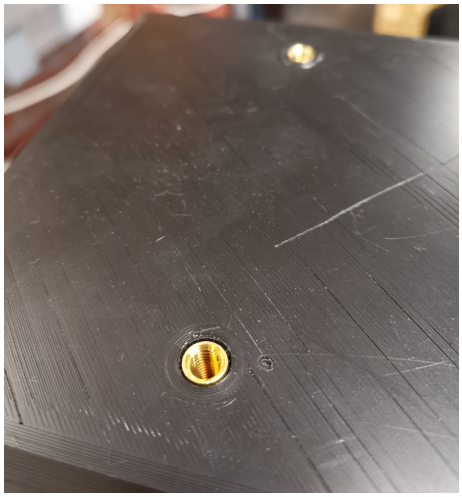

Figure 5.4: M6 screw insert melted into the upper middle part of the bus model

Figure 5.5: The magnets that hold the front and rear part together with the center of the bus

5.1.5 Surface Treatment of the 3D Printed Parts

When the parts have been 3D printed, and in some cases glued together, the irregularities and joints of the parts needs to be filled out. This has to be done to get a smooth surface, which means a low skin friction factor on the surface of the bus when the model is tested in the wind tunnel. When the filler has hardened it is sanded down so only the necessary part of the filler is left and desired smoothness is achieved. How it looks when the filler has hardened can be seen in figure 5.6.

Figure 5.6: Part of the bus model where filler have been applied

When a satisfactory smoothness of a part has been reached a layer of spray filler is applied to the part to get a homogeneous surface. In this way the paint that will be applied will have the same surface to stick to and the result will be the same all over the model. When the spray filler has dried it was sanded down with a fine sand paper to a smooth surface, this can be seen in figure 5.7.

Figure 5.7: The bus model with spray filler applied

When the part has a smooth homogeneous surface it is painted with black spray paint as seen in figure 5.8. This was done to get a similar skin friction coefficient as on a real bus. The colour black is chosen to give a good contrast when using smoke and tufts in the wind tunnel, due to that the smoke and tufts used are white.

Figure 5.8: Parts of the bus model with paint applied

When all parts have gone through all the steps of the process they are assembled together. The final model can be seen in figure 5.9.

Figure 5.9: Assembled bus model with completed surface treatment

5.2 Mounting the Bus in the Wind Tunnel

In this section the process of the installation of the scaled bus model in the wind tunnel explained.

5.2.1 Designing the Mounting Device

The model of the bus needs to be positioned on a scale in the wind tunnel, which can measure forces and moments in all directions. The chosen scale was one that could be rotated around the z-axis, as shown in figure 5.10. With this scale it is therefore possible to investigate many different yaw angles in short period of time.

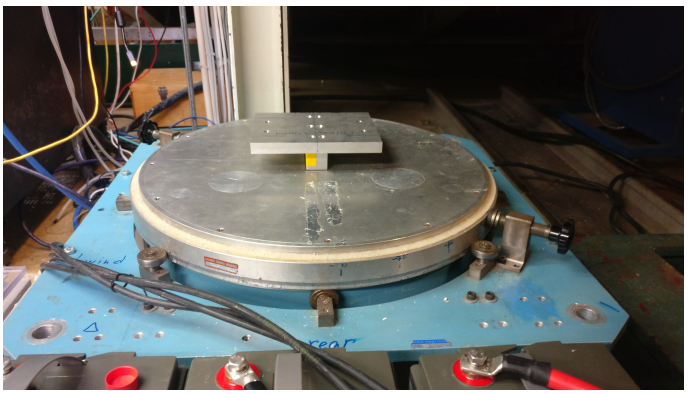

Figure 5.10: Scale that is used in the wind tunnel

To get correct and easy to work with results some aspects needed to be taken into account. First and most important is that the forces acting on the scale should only come from the drag on the bus. This is achieved by having rods going up from the scale that is placed below the wind tunnel, through holes in the floor and then connected to the wheels as seen in figure 5.11. It is important that the rods do not have physical contact with the floor of the wind tunnel, if that is the case, the forces acting on the model will be transferred to the ground instead of the scale. Second thing to have in mind is the placement of the bus relative to the scale. To have easy results to work with, the center between the wheels of the bus should be aligned with the center of the scale in the z-direction as illustrated with the dashed line in figure 5.11.

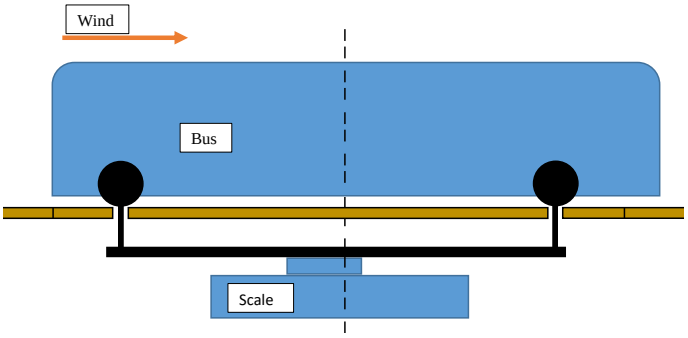

Figure 5.11: Illustration of how the bus model is attached to the scale. The wheels or rods do not have contact with the ground plate

Measurements were taken of the scale, the wheelbase and track width of the bus. With this a drawing of the adapter plate between these two were made, shown in appendix A.1. For the existing ground plate in the wind tunnel that was used an insert needed to be made that can be rotated with the holes for the rods going up to the wheels. As illustrated in figure 5.12 the plate has a square cut out over the hole, $3mm$ deep. The rotating insert can therefore have an edge that rests upon this cutout without interfering with the flow, the leftover area around this is filled with a masonite board to be flush with the rest of the ground. For easy visibility of the yaw angle used in the tests an indicator is printed on top of the rotating insert.

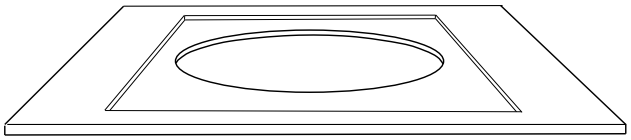

Figure 5.12: Illustration of the ground plate in the wind tunnel

5.2.2 Building the Mounting Device

In the building of the adapter plate and the ground, the Chalmers workshop was used. Chalmers also supported the build with materials that was available in the workshop. The drawings were made in a way that had some freedom in what materials that were used, as long as tests of the deflection of the mounting plate with the force calculated in section 5.1.1 and controls that the deflection does not create interference between the ground and scale. The interference is that one between the rods to the wheels and the holes in the ground.

For the adapter plate a $3mm$ thick sheet of metal was used. The use of a single sheet made it easy to, with a high level of accuracy, mark out the holes for screws and rods, to make it more rigid a steel profile were welded to the surface as seen in figure 5.13.

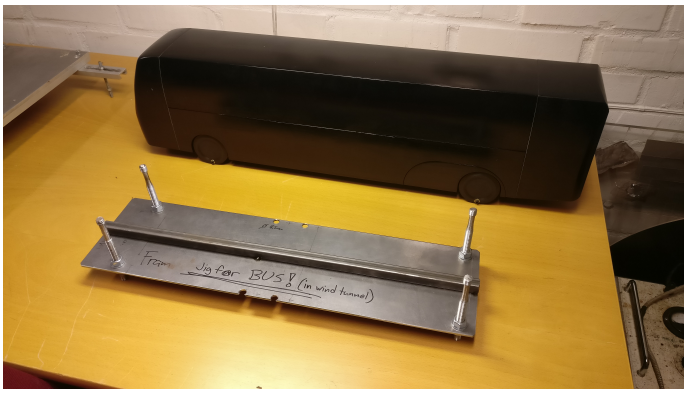

Figure 5.13: The adapter between the scale and the bus wheels

For the rotating part of the ground plate a $12mm$ thick form plywood was cut out with a router that was attached to a center hole in order to get a perfect circle. The $3mm$ high edge that sits on top of the aluminum plate was cut out with the same technique as shown in figure 5.14.

Figure 5.14: Cutting out an edge on the rotating plate with the router

The same setup with the router was used to make the masonite board that fits around the rotating plate. In figure 5.15 the underside of the finish setup can be seen and in figure 5.16 it is installed in the wind tunnel.

Figure 5.15: Rotating plate inside the masonite board

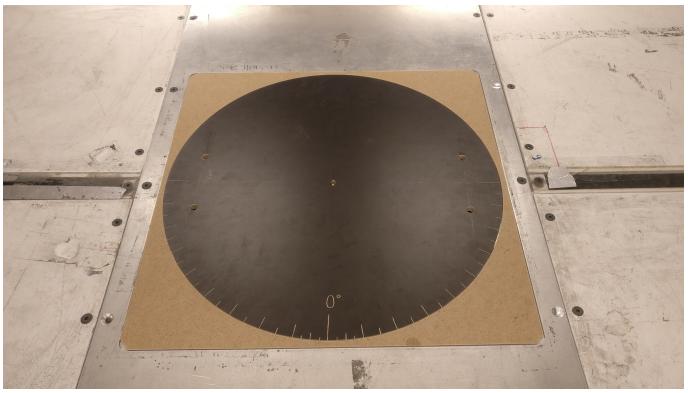

Figure 5.16: Finished setup of the ground in the wind tunnel

5.3 Test Preparations and Execution

The time available for the tests in the wind tunnel was two days. In this time the bus should be installed in the tunnel, a full positive and negative yaw angle sweep should be done and after that analyse of the flow with different techniques. This meant that a detailed planning was needed, to make sure that all planned tests were performed.

First of all a Reynolds-sweep was made to see at what wind speed the tests should be made. A Reynolds-sweep is when you calculate Cd for different wind speeds and then look for the speed were it is not changing to much. This speed became $35m/s$ as seed in figure 5.17.

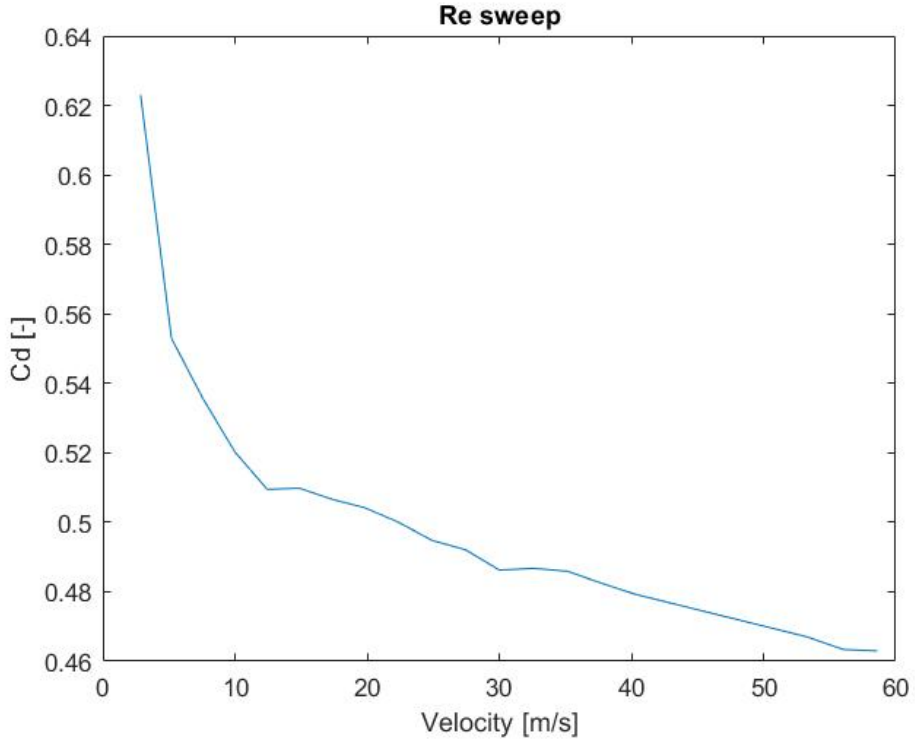

Figure 5.17: Reynolds-sweep of straight forward facing wind on the bus model in the wind tunnel

For the different yaw angles it was planned to go with steps of 2.5° up to the yaw angle of 10° and after that in steps of 5° up to 90° which is complete side wind. Then after that the size of the steps was 10° until a yaw angle of 180° which is straight rear facing wind. All this for a positive and a negative sweep to also investigate symmetry of the model and setup. The full test plan for the wind tunnel can be found in appendix A.1.

The point of doing a complete sweep of angles is to get measurements of forces and moments around x, y and z-axis. The data from the scale is therefore saved in a text file in a number of columns, these columns needs to be identified and sorted in order to extract the values that later is plotted in graphs. To do so a script in Matlab was written that can be used to make the graphs while the tests is conducted. In this way it is easy to see if the data is corrupt and changes needs to be done to the setup before continuing the process. The process itself of conducting one test is listed below.

- Set the correct angle
- Check so the rods and bus don't touch the ground
- Make sure that the wind speed is zero
- Zero the scale
- Start the wind tunnel and wait for the wind speed and measured values to stabilize
- Save the values from the scale and the actual wind speed
- Stop the wind tunnel and prepare for next test

After the sweep of angles the investigation of the flow was made, for this, three techniques were used, smoke, thermal camera and tufts. The tufts were on the bus during the sweep and works on

default. To create the smoke, oil is vaporized and directed to where you want to investigate the flow.
When using the thermal camera the side of the tunnel will be open so that the heat that the lamp emits will hit the bus without obstruction, the light and camera configuration is shown in figure 5.18. The surface of the bus will be heated from the lamp and then cooled down where the flow of air is high. This temperature difference is captured with a thermal camera.

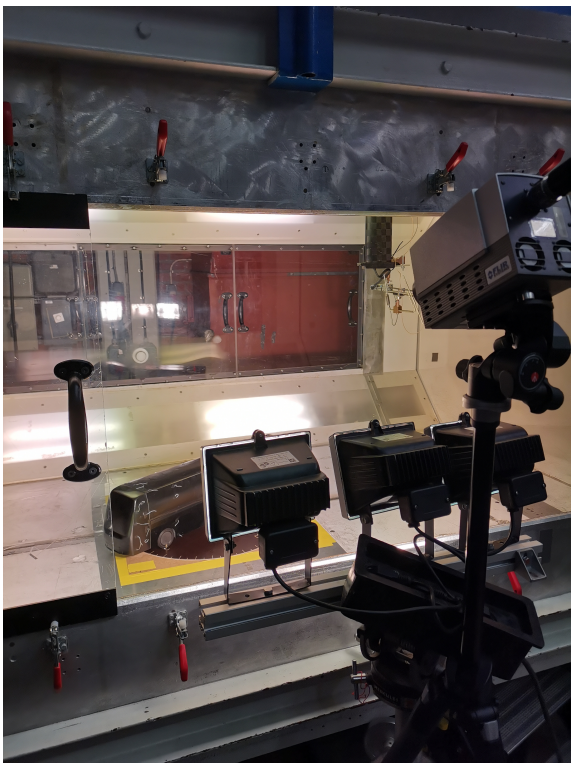

Figure 5.18: Setup of the thermal camera and the lights

6 Results

In the following chapter, the data from the wind tunnel and the simulations are shown together with discussion and comparison of the results. Areas that are of a special interest in regards to the deviation from trends or areas of interests for stakeholders are analysed further more.

6.1 Resulting Forces From Wind Tunnel and CFD

Simulation performed in CFD covered a case when the real road conditions were imitated. The difference between the wind tunnel tests and the simulations are that in the wind tunnel there is no moving ground, the wheels are not rotating and blockage effects. Also the Reynolds number is not the same in both CFD and wind tunnel. In order to compare the results, the non-dimensional coefficients for forces and moments acting on the bus were plotted, together with results obtained from the wind tunnel and displayed in figures 6.1 to 6.9. The main goal was to identify similar trends for wind tunnel tests and simulations.

6.1.1 Coefficient of Lift

The first force coefficient presented is coefficient of lift in figure 6.1. One can observe that there are some areas with extensive positive Cl and some with negative Cl. The positive Cl creates lift whereas, the negative values represent generated down force. It can be observed that at 0° yaw angle conditions the bus experiences a little bit of down force due to negative Cl coefficient, roughly around -0.2. When the yaw angle reaches approximately 10° there is a lift force generated both noticeable in the CFD and the wind tunnel outcomes. The further development of the Cl trend after 10° suggests that the velocity magnitude increases around roof region in comparison to the underbody velocity from $10 - 40°$. The result of this is that lift is created. Consequently the circumstances change, after its peak of $Cl = 1.2$ at 35° the Cl begins to decrease and even becomes negative from 67.5° thus the bus experiences down force.

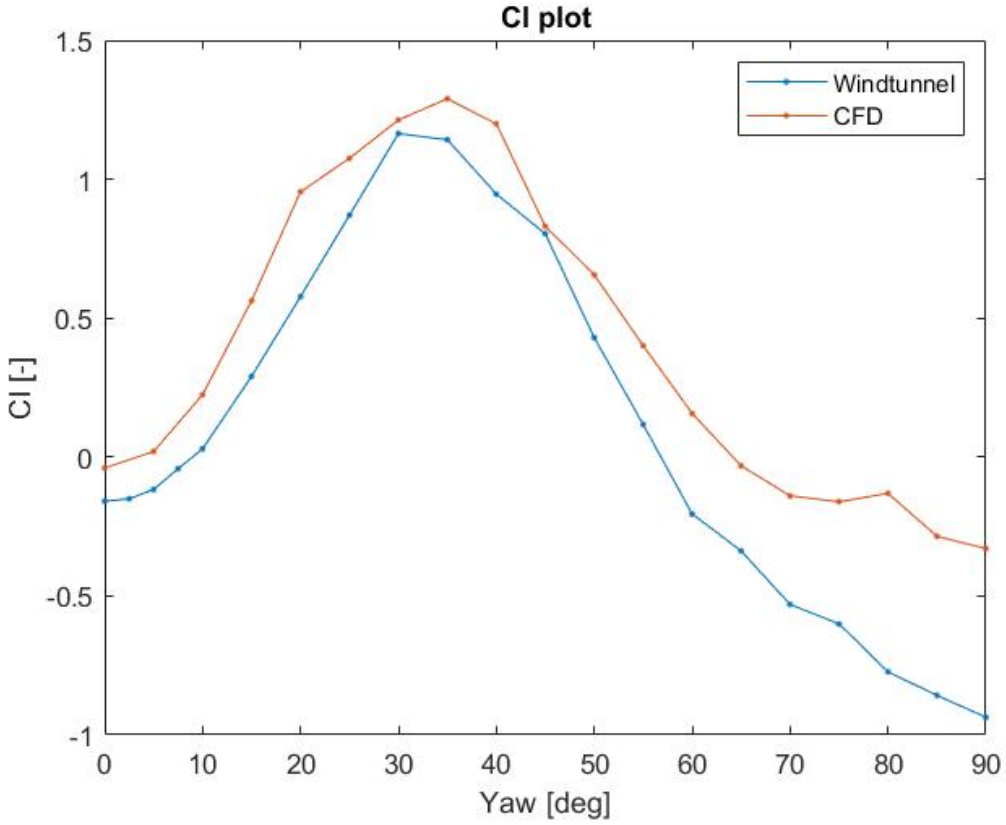

Figure 6.1: Comparison of lift force coefficient between the wind tunnel and CFD

Furthermore, comparisons were made with contour plots of the velocity taken at 30° and 60°. At 30° yaw angle there is a peak in Cl that makes this point interesting. The cause of this peak in lift is due to high speed wind interaction with the roof of the bus and and low speed wind under the bus as seen in figure 6.2. This creates low pressure on the roof and high pressure under the bus which is similar to what happens with a typical aerofoil. On the other hand, in the case of 60° yaw angle the wind speed decreases in roof regions and unlike previous case, the underbody wind speed increases thus resulting in down force. Also at 30° yaw angle, down wash can be observed from the roof of the bus to the left side of the bus in figure 6.2 which results in contribution to lift force. This down wash is not observed at 60° yaw angle because of separation on top of the bus. Separation on top of the bus is one of the reasons for the decreasing trend in the Cl plot in figure 6.1 after peaking at around 30°.

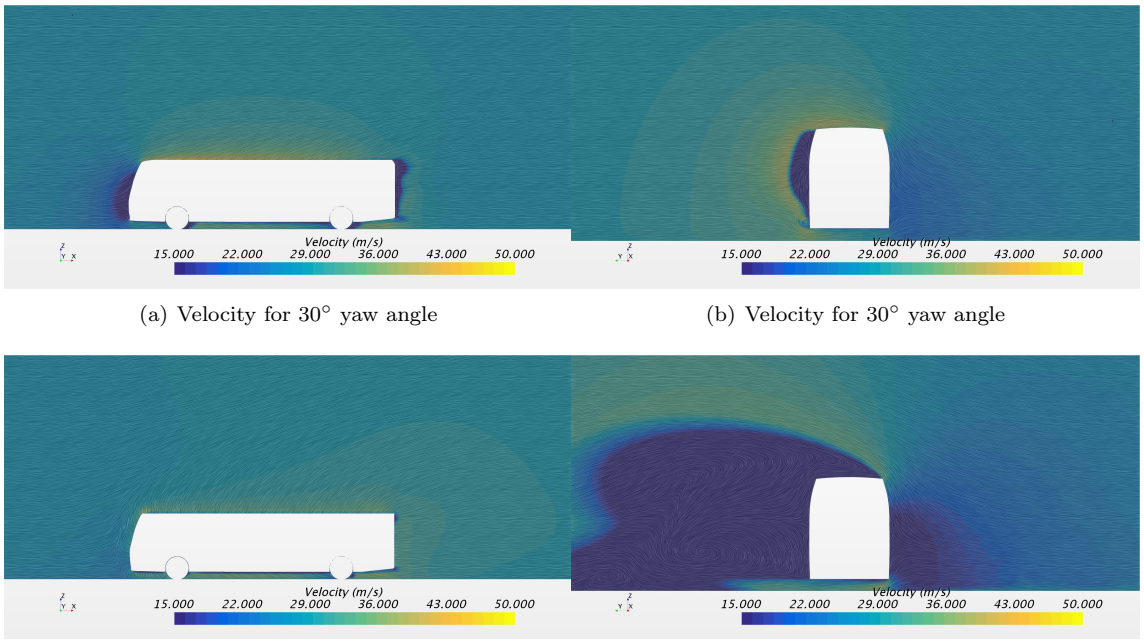

(a) Velocity for 30° yaw angle

(b) Velocity for 30° yaw angle

(c) Velocity for 60° yaw angle

(d) Velocity for 60° yaw angle

Figure 6.2: Velocity plots for different yaw angles

6.1.2 Coefficient of Drag

When inspecting the results of drag, Cd, in figure 6.3 the trend is similar to lift. The results from simulations and wind tunnel tests are not exactly the same but show a similar trend. This could be because of the not having rotating wheels or moving ground in the wind tunnel. In the beginning, there is a sudden increase, which would indicate high difference in front and rear pressure. However, around 25° the trend reverses again and continues to decrease until around 75° were it starts to go back to zero in drag at 90°. On top of that, since the vehicle used in this project is a bus the friction drag cannot be neglected, however it's effect will be more discussed in the section Analysis of flow patterns.

The important angle in terms of drag is 60°, here the drag is zero and starts to go to negative values. The reason for this phenomenon can be drawn from figure 6.4 that shows velocity and pressure coefficients. Since the main component of the drag is pressure drag, the stagnation areas and wake regions play an import role. The values of drag are caused by the difference of the pressure in frontal stagnation area and in the wake, that is characterized by high velocity and low pressure, which can be observed from picture b in figure 6.4.

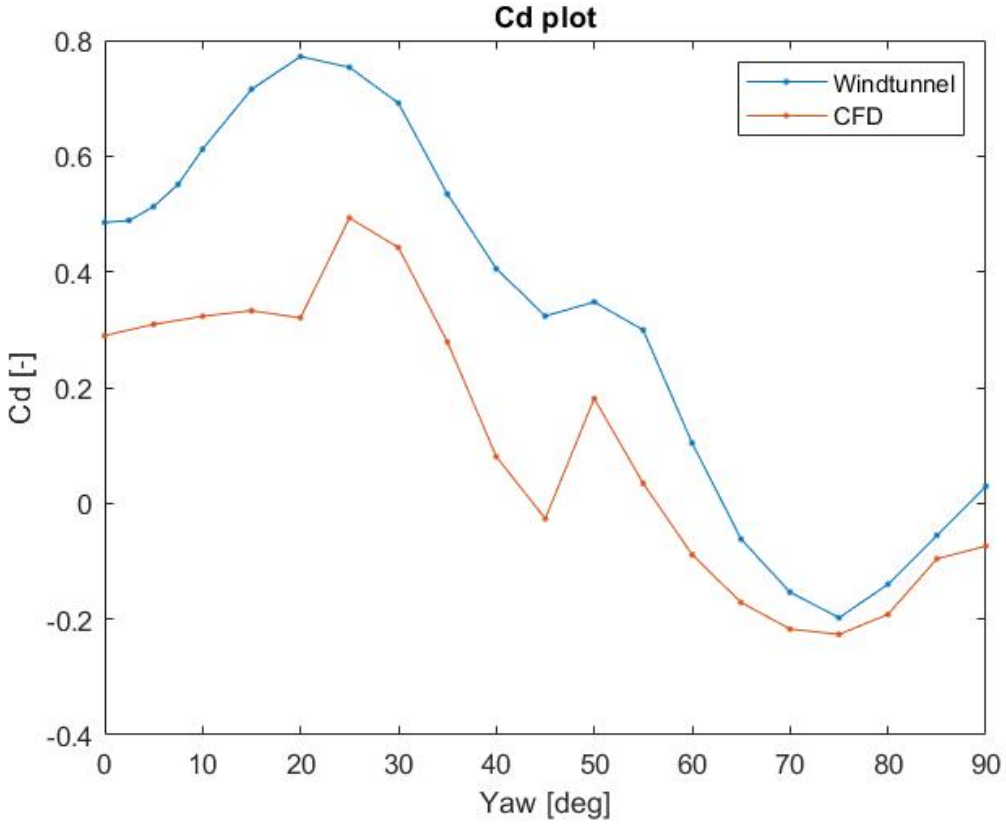

Figure 6.3: Comparison of drag force coefficient between the wind tunnel and CFD

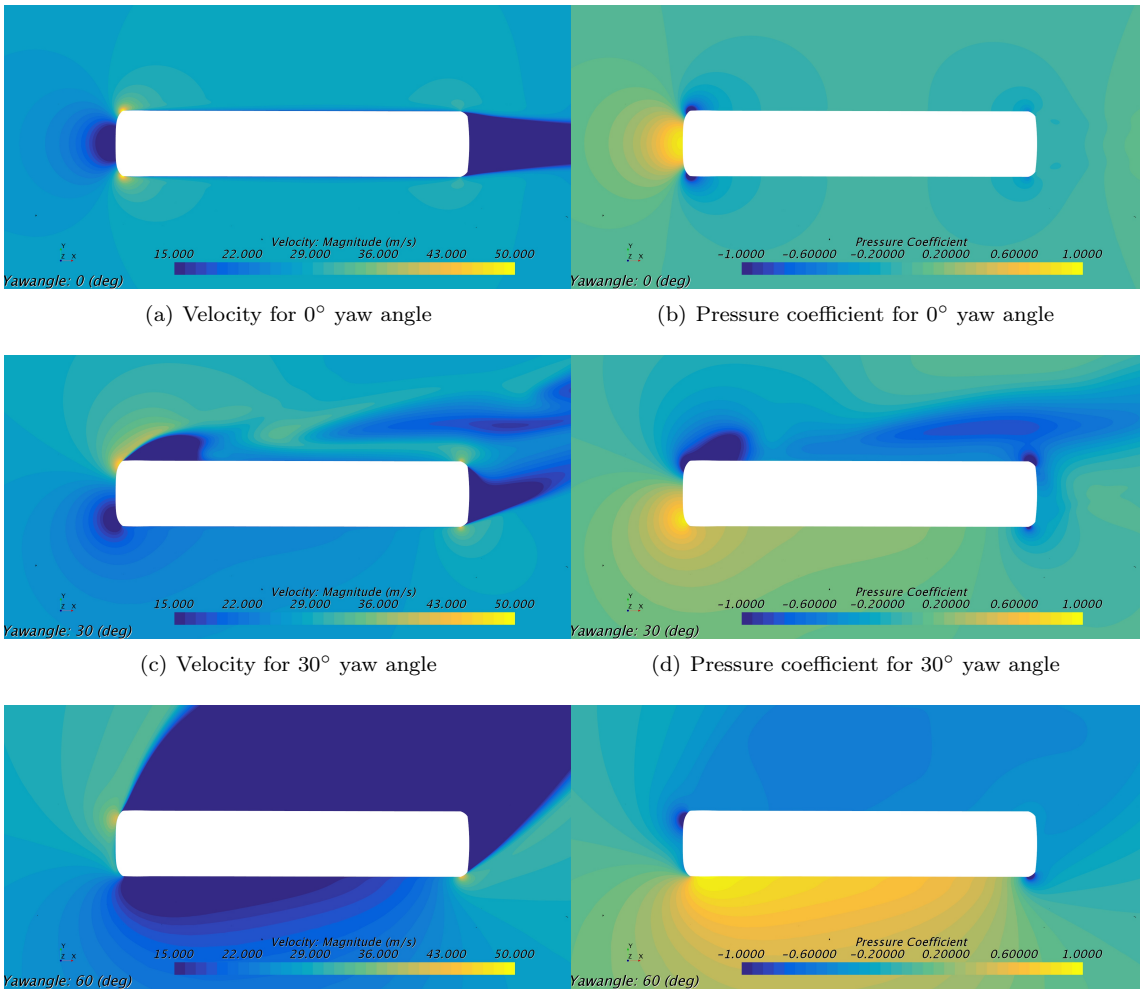

(a) Velocity for 0° yaw angle

(b) Pressure coefficient for 0° yaw angle

(c) Velocity for 30° yaw angle

(d) Pressure coefficient for 30° yaw angle

(e) Velocity for 60° yaw angle

(f) Pressure coefficient for 60° yaw angle

Figure 6.4: Velocity and pressure plots at a plane 1.5m from ground

6.1.3 Coefficient of Side Force

When observing the coefficient of side force acting on the side of the bus, Cs, there is an obvious trend that the force is increasing with a increase in side wind as seen in figure 6.5. From 0° to 45° the increase is almost perfect linear and can therefore be described with a linear equation. But after 45° the force starts to stabilize and can almost be assumed constant until 90°. In figure 6.6 the reason why the force is constantly increasing is clearly shown with help of the increasing intensity of the colour yellow on the side of the bus. This indicates an increasing pressure on the side of the bus between 0° and 90° of yaw. From angles 60° to 90° the increase in the pressure on the side of the bus is not as much as for angles lower than 60° and that is why the plot stabilizes beyond this yaw angle. The maximum side force observed for full scale bus in CFD was 19780N which was 1.5 times greater than the maximum drag force and almost 4 higher than the maximum lift force. This shows that forces acting along the side of the vehicles with large side areas is far more greater than the forces in other directions.

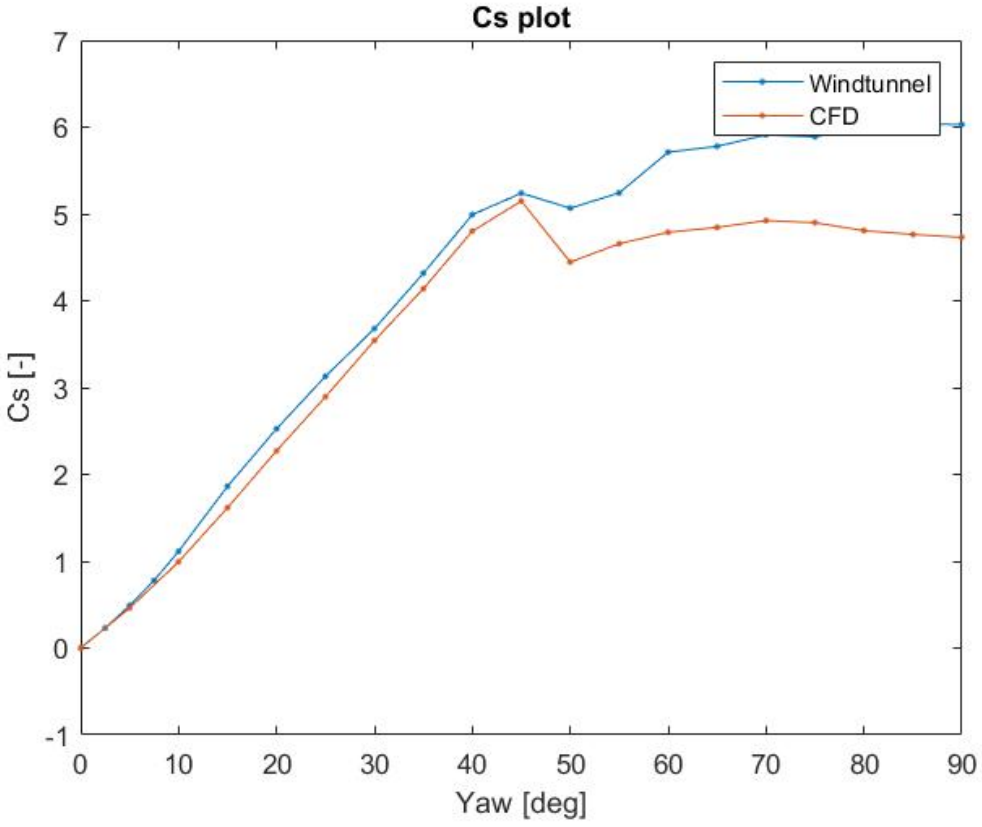

Figure 6.5: Comparison of side force coefficient between the wind tunnel and CFD

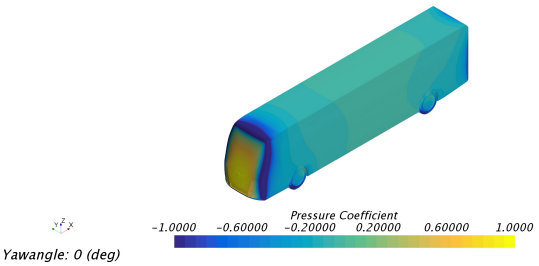

(a) Pressure coefficient for 0° yaw angle

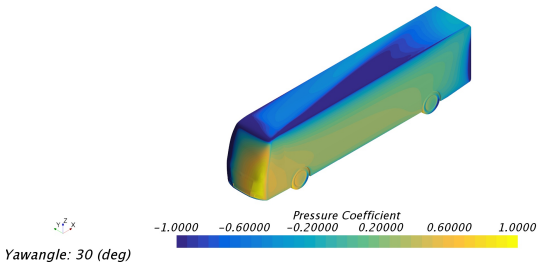

(b) Pressure coefficient for 30° yaw angle

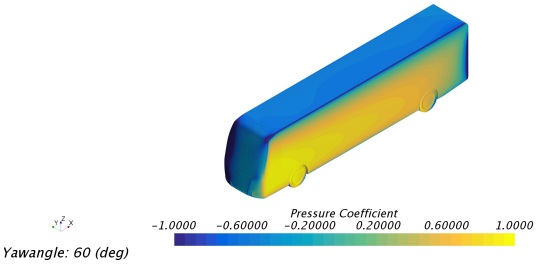

(c) Pressure coefficient for 60° yaw angle

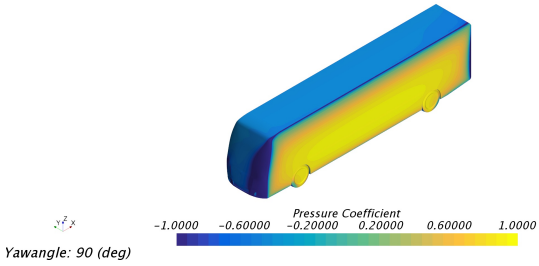

(d) Pressure coefficient for 90° yaw angle

Figure 6.6: Pressure coefficients for different yaw angles

6.1.4 Coefficient of Moments

Regarding the moments acting around the x, y and z-axis the trends of CFD corresponds well with the wind tunnel as seen in figure 6.7 to 6.9. On the other hand the difference in magnitude of Cmx and Cmy between CFD and wind tunnel is more then two times higher in wind tunnel. This is due to were the coordinate system is placed that the moments are measured around. In the CFD-simulations the x-axis and y-axis are flat on the ground meanwhile in the wind tunnel they are around $160mm$ beneath the ground inside of the scale. This creates a longer moment arm in the wind tunnel and therefore a greater moment around the axis. When later being applied in a vehicle model it is of great importance to know how the data where measured. For the moment around z they correspond better due to that they are aligned through the same point on the bus in CFD and in the wind tunnel.

It can observed from figure 6.7 that the roll moment coefficient, Cmx, increases in both CFD and windtunnel until 45° quite sharply and then slowly increases to a maximum value at 90°. Roll moment coefficient effects the weight distribution in lateral direction. Increase in the value of roll moment increases the instability of the vehicle as it will tend to overturn. Further it can also be observed that the plot in figure 6.7 and figure 6.5 the trend is similar. This implies that the increase in side force is the cause for increase in the roll moment acting on the bus.

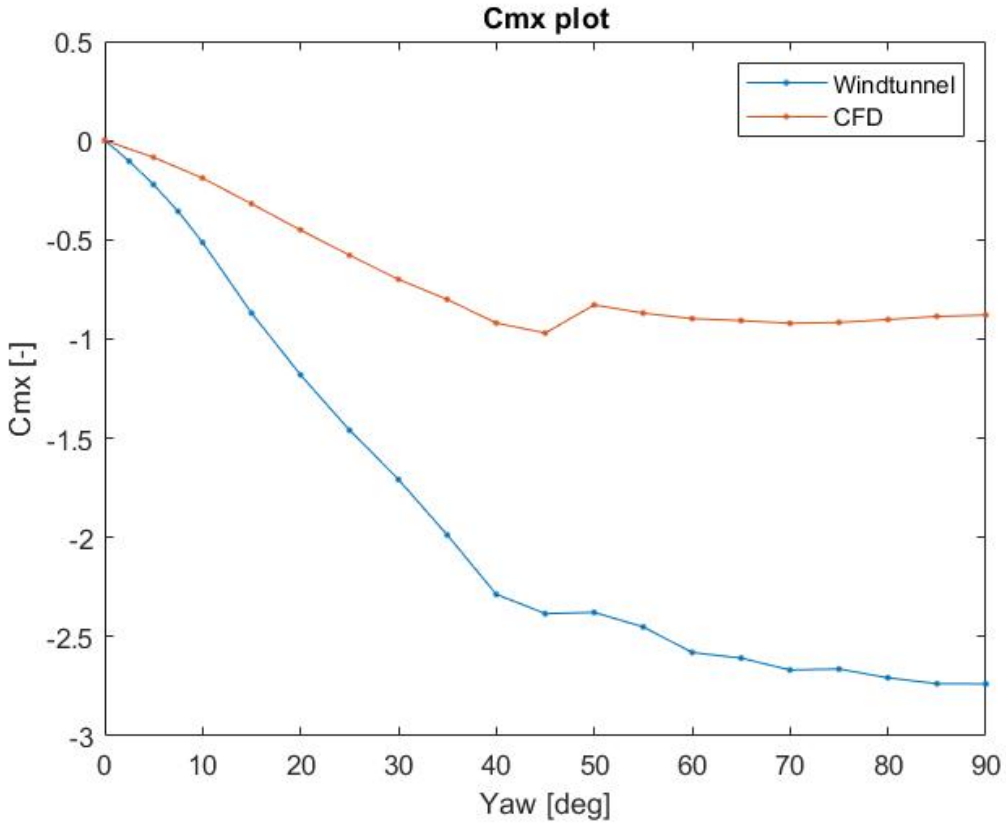

Figure 6.7: Comparison of roll moment between the wind tunnel and CFD

Figure 6.8 shows the effect of yaw angle on the pitching moment of the bus. Pitching moment increases until 40° before dropping steeply and changing direction at close to 60°. Pitching moment effects the vehicle weight distribution in the longitudinal direction, i.e. the load shifts from one axle to another. However the magnitude of this coefficient, when compared to other coefficients,

is small. This indicates that the the load transfer from one axle to another is not as significant as other load transfer in other directions.

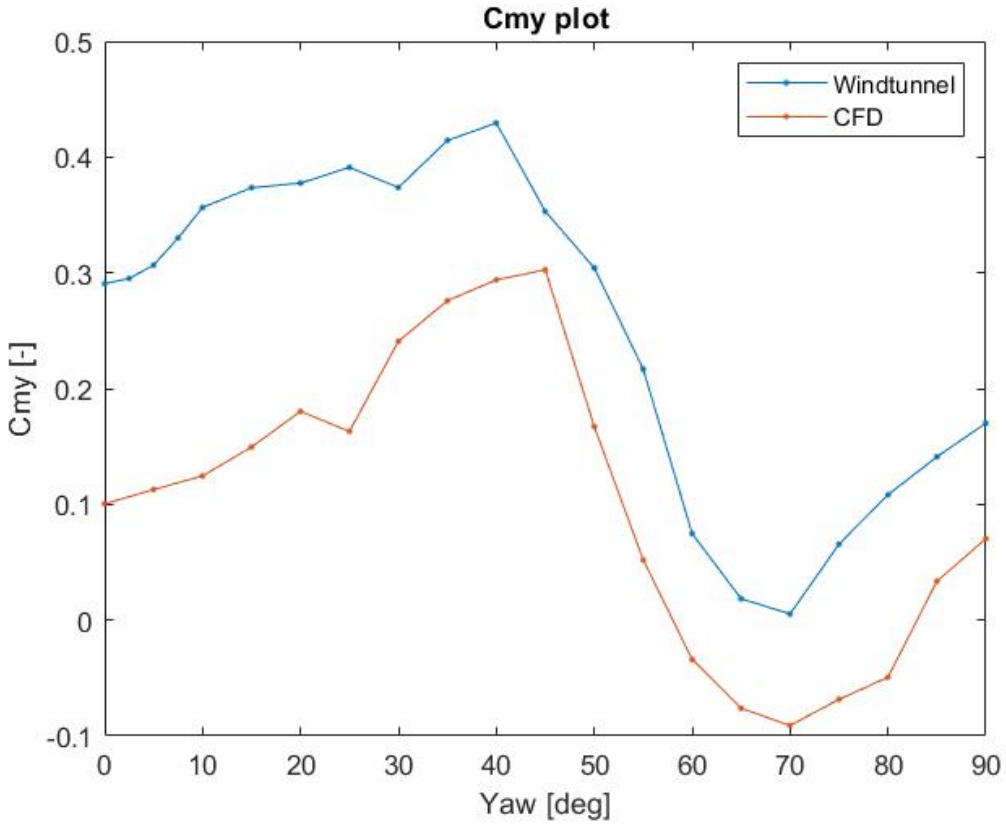

Figure 6.8: Comparison of pitch moment between the wind tunnel and CFD

It can be observed that the yaw moment coefficient of the bus increases with the yaw angle until 45° and then decreases all the way to the end in the figure 6.9. Yaw moment is an important parameter as it is used to describe the ability of the vehicle to stay in its straight path while driving i.e. directional stability of the vehicle. Velocity vector field at a plane 1.5m from ground in figure 6.10(a) shows that the flow reattaches at yaw angle of 45°. However it can be observed in figure 6.10(b) at 60° yaw angle the flow is separated completely which acts as an opposition to the yawing motion of the bus. This is the reason why the yaw moment coefficient decreases beyond 45°.

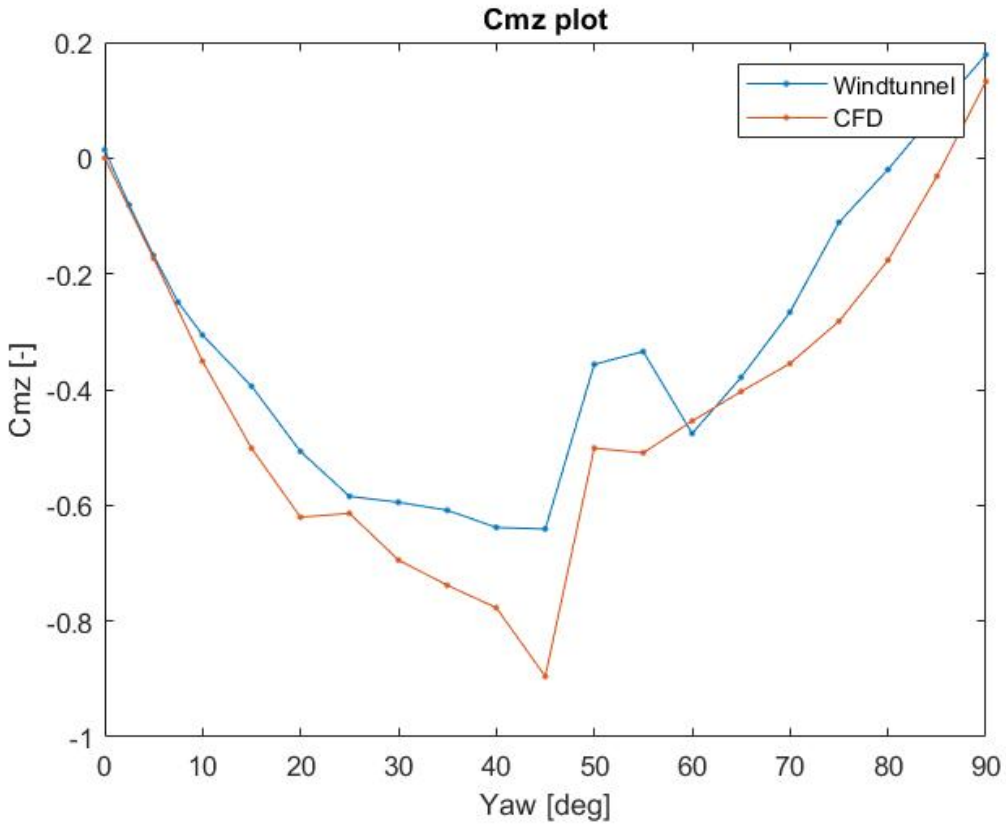

Figure 6.9: Comparison of yaw moment between the wind tunnel and CFD

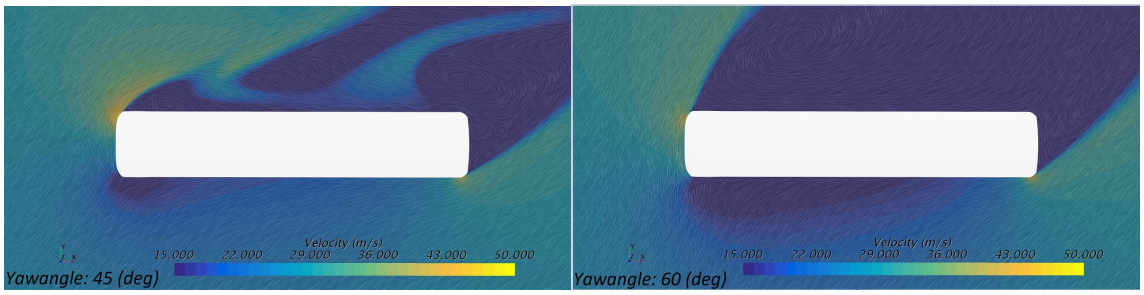

(a) 45° yaw angle

(b) 60° yaw angle

Figure 6.10: Velocity vector fields at a plane 1.5m from ground

A sharp change in trend of a plot can be observed in the figures 6.3, 6.5, 6.7 and 6.9 from 45° to 50°. This sharp change can be explained using figure 6.11. There is some acceleration of flow around the front and it re-attaches itself after a small amount of separation at three different heights of 0.5, 1.5 and 2.7 m from the ground. This acceleration is reduced due to complete separation of flow on the leeward side of the bus for yaw angle of 50° at all the heights mentioned before. Separation on leeward side of the bus changes the pressure distribution around which contributes to the change in the resulting forces and moments.

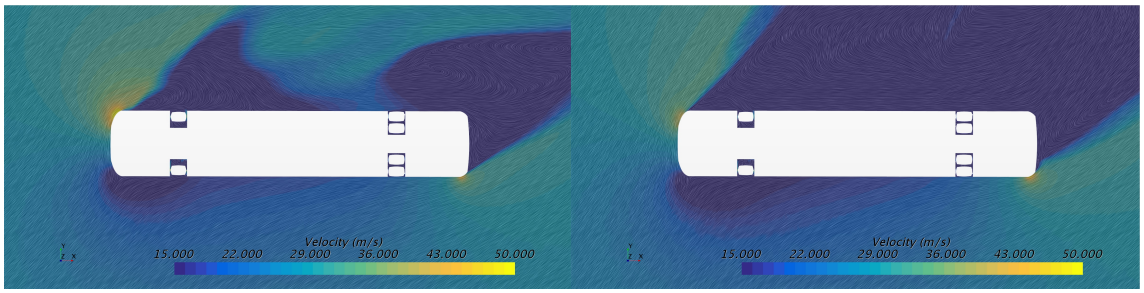

(a) 45° yaw angle at 0.5m from ground

(b) 50° yaw angle at 0.5m from ground

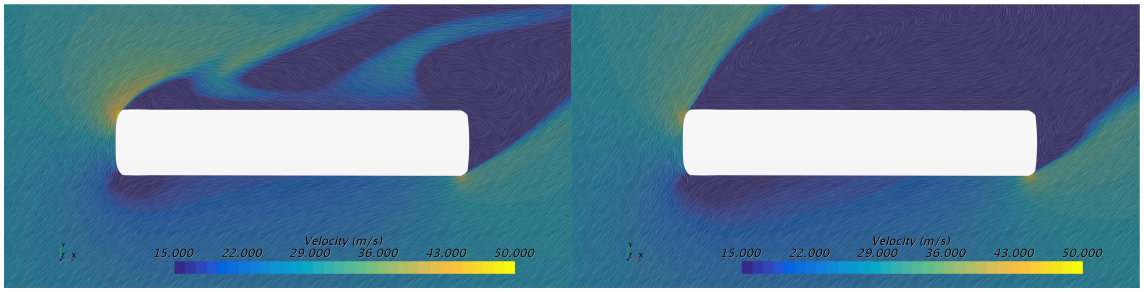

(c) 45° yaw angle at 1.5m from ground

(d) 50° yaw angle at 1.5m from ground

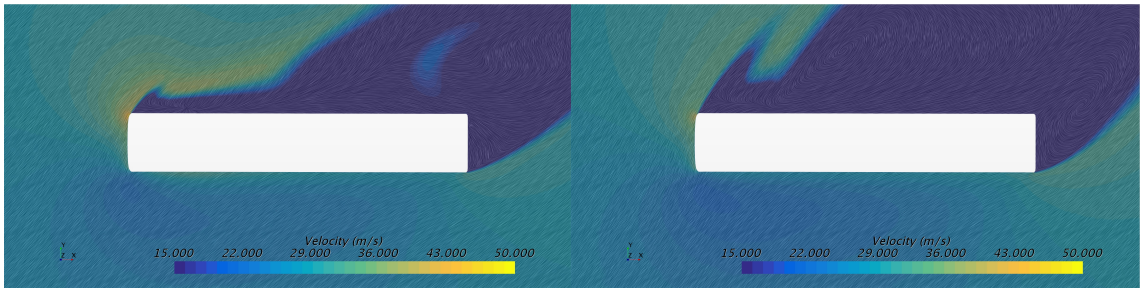

(e) 45° yaw angle at 2.7m from ground

(f) 50° yaw angle at 2.7m from ground

Figure 6.11: Velocity vector plots at different heights from ground

The results discussed shows a good agreement in terms of trends in behaviour of bus between CFD and wind tunnel tests even with the differences mentioned earlier.

6.2 Analysis of Flow Patterns

The pictures taken by the thermal camera show how the air moves around the bus close to the surface and can reveal areas that contribute more or less to skin friction drag. For the general flow around the bus the smoke is used to analyse the flow. These pictures will be analysed in this section.

From figure 6.12 the vortex on the down stream side of the bus can be seen by analysing the cooler areas. When the air flows over the bus it separates at the edge of the roof, then it goes down and hit the side in the middle where it cools down the surface and therefore creates the black area along the middle. Same can be seen at a small vertical section right in front of the front wheel were the air that have released from the A-pillar reattaches again. The bright white area at the top of the side indicates a wake region with a small amount of moving air at an average.

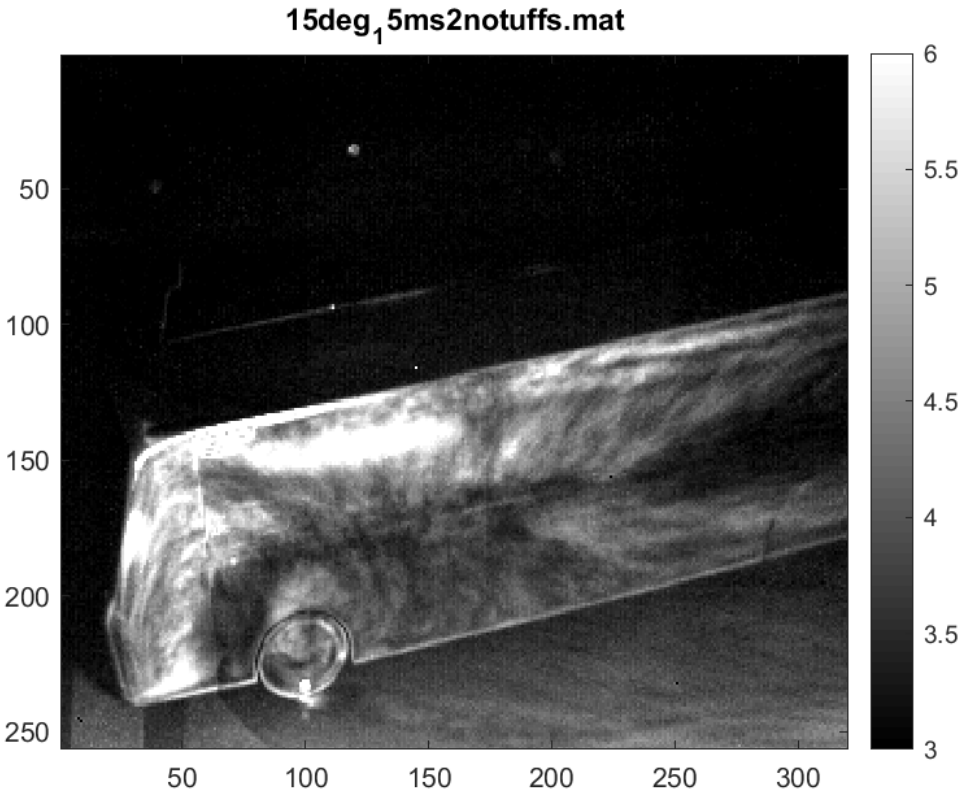

Figure 6.12: Thermal camera picture at 15° yaw angle

The smoke was used at 30° yaw angle, which is where the bus experience maximum of lift according to figure 6.1. In figure 6.13 below the smoke can be seen going from ground level all the way up and over the bus. This explains the low pressure on the roof and why there is a peak in lift.

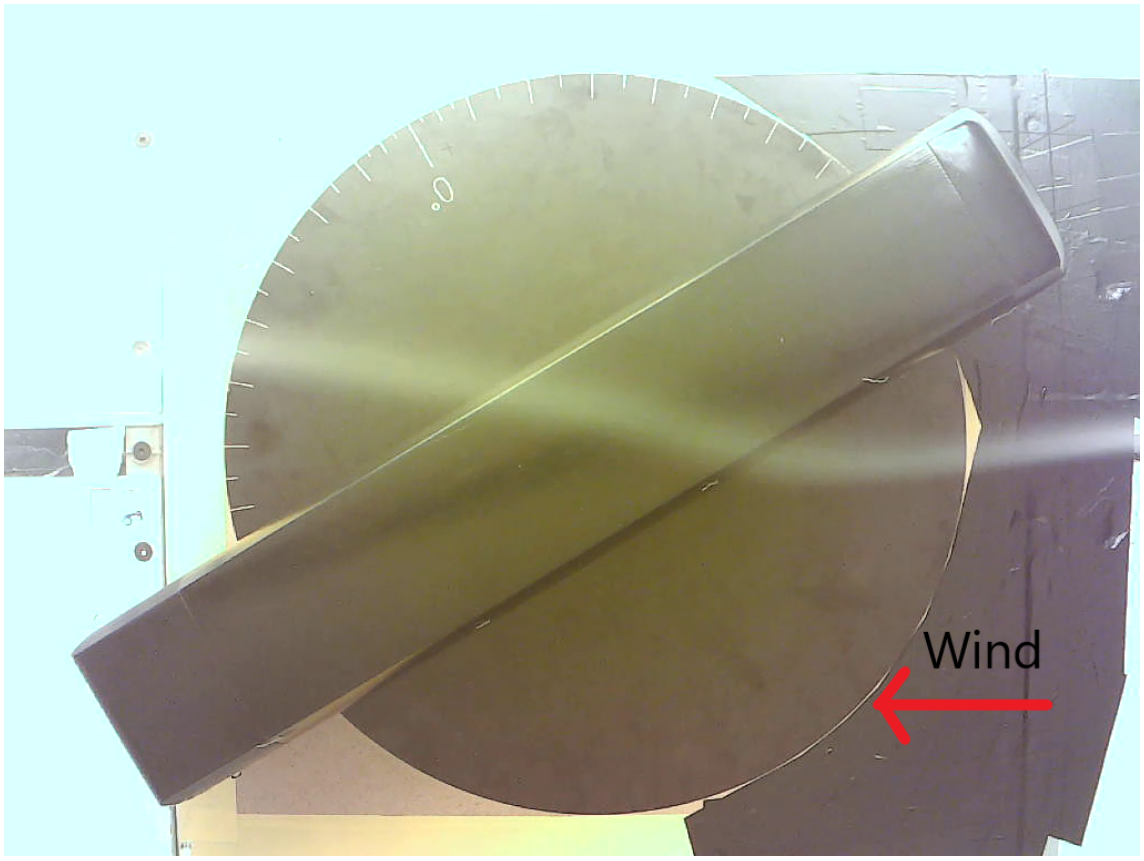

Figure 6.13: The flow of air over the bus from close to ground level at 30° yaw angle

To see the flow closer to the surface of the bus a picture with tufts is shown in figure 6.14. Here it can be seen that more air moves over the bus then under the bus according to the tufts in the front. Only the one furthest down indicates that air goes under the bus, the rest of them show flow along the bus or up to the roof. How the air separates after the edge can not be visually confirmed to prove that it is attached like it is in picture b in figure 6.2. In order to improve visualization of where the flow is attached new tests with more tufts located closer to the edge on the roof needs to be made.

Figure 6.14: Tufts that show the flow of air close to the surface of the bus at 30° yaw angle

7 Discussion and Interpretation of Results

Exporting the original surface model from Ansa to a format usable in Catia was a compromise in regards to model adjustability. When importing a model the information about individual features is lost. The model consists of a number of individual surfaces without any links to each other. To make a solid from surfaces in Catia one manifold surface must be used, so the individual surfaces must be joined before. Unfortunately wide gaps between a lot of the panels of the model made it cumbersome to use the original model. A new model was therefore created in Catia using the Ansa model as the reference.

It is possible to argue that a bus model in scale 1:18 is large enough not to be suitable for 3D printing. Because of the rather simple geometry of a bus making the model using a computer numerical controlled (CNC) mill could both make it faster and more detailed. Another advantage would be the amount of after treatment that would be needed for the surface to achieve a smooth surface. Machined surfaces can, depending on model material, have a very good surface finish without any further process. If no finishing process is needed the amount of time of manual labor is greatly reduced as well as an increased accuracy in getting a completely symmetrical model. The fact that the model became modular makes it more reasonable to 3D print since it needs to be concluded of several parts regardless of production method. In the end a 3D printer was used instead of a mill due to availability and ease of use to the project group.

The simplifications made to the bus model used in this project such as the removal of the mirrors and a flat floor could of course effect the end result. Though this is most likely only true for when the wind is attacking the bus from the front, when the bus is faced with heavy cross wind from the side it is very unlikely that the simplifications makes a noteworthy difference because of the very large side area. Since this project aimed to investigate heavy side wind conditions it was concluded that a simpler model would save time for both the CFD simulations and the scale model build.

Two factors that would actually make a large difference would be to have moving ground and rotating wheels, as these affects the air flow around the bus quite much. Since the scale model had to be mounted on top of struts protruding out of the ground of the wind tunnel the ground clearance is also increased compared to the simulated bus. If moving ground and rotating wheels would have been present in the wind tunnel during testing it is possible that the results would better correlate to the ones that came out from the CFD simulations. It is also worth noting that the wind tunnel at Chalmers is not equipped with boundary layer suction, in the optimal case this would be added in addition to the moving ground and rotating wheels.

Regarding the thermal camera results found in the report, the picture are there to show the capability and usage area of the camera. If further test were to be done some improvements of the setup would be preferred. Such as the position of the camera and the light source that produces both light and heat. This should be done to improve quality of the pictures and easier see the path of the airflow around the bus. One issue right now is that the camera and lights are standing outside the wind tunnel, which means that the wind tunnel sides needs to be open in order to get the heat from the lights to the model in the wind tunnel and not obscure the camera view with glass. This means that a lot of air escapes the wind tunnel trough the open side and the escaping airflow onto the equipment makes the camera vibrate and makes it hard for the camera to focus. The open side of the wind tunnel creates a limiting factor since it limits what wind speeds that is possible to run during the tests.

The results from CFD and wind tunnel followed a similar trend which enabled us to draw some conclusions on the effects of side winds on a bus. The CFD study made by William Y.E. et al [1]

until 45° yaw angle shows similar trends to the results presented. However, the absolute values of forces could not be compared as the CFD setup and model of the bus are different in both the studies. The absolute values of the forces and moments cannot be taken as output from this study as both wind tunnel and CFD had its own limitations. In CFD RANS equations with a simple turbulence model was used which gives mean fields as solution and models turbulence without resolving it. Running detached eddy simulations (DES) or similar could result in solutions much more realistic than in the present case. The wind tunnel test is made on scaled down model, without moving ground and rotating wheels which makes the results less accurate. Hence, we can take a conservative approach and make conclusions on general trends in the present study.

8 Conclusions

From the two days in the wind tunnel the conclusion drawn were that the test plan created could be followed as planned and more tests could be performed due to that the mounting of the bus in the wind tunnel went quicker than expected. If the wind tunnel test had been performed later in the project, the results from the CFD simulations could have been taking into account when planning the tests. Using the findings from the conducted sweep an additional wind tunnel testing session could have been performed in order to further evaluate the areas of interest.

Simulating the impact of the side wind on the bus in CFD was also an important part of the project. Numerous strategies were implied in terms of mesh selection, physics and solvers. When the results were compared to the measured data from the wind tunnel, clear similar trends were spotted in plots of all major force coefficients and moments. An increasing trend in side forces and roll moments with yaw angle could be observed in both CFD and wind tunnel. This shows that at high angles of yaw, the resulting aerodynamic forces and moments play a crucial role in stability of the vehicle and highlights the importance of such a study. The other forces and moments also gave useful information on its dependency on yaw angle. These forces and moments peak at lower angles and have less effect on vehicle stability when compared to the side force and roll moment.

It can be concluded that the data collected from the project can be seen as reliable, as both the wind tunnel tests and the CFD simulations correlate well. Since the wind tunnel data is from a scaled model and the CFD simulation were done on a simple numerical model the results should be analysed with caution using a conservative approach.

References

[1] Youhanna E. William, Mohamed H. Mohamed and Walied A. H. Oraby. *Investigation Of Cross-wind Aerodynamics For Road Vehicles Using CFD Technique*, Eleventh International Conference of Fluid Dynamics, 2013.

[2] L. Salati, P. Schito, D. Rocchi, and E. Sabbioni. *Aerodynamic Study on a Heavy Truck Passing by a Bridge Pylon under Crosswinds Using CFD*, American Society of Civil Engineers, 2018.

[3] Huoyue Xiang, Yongle Li, Suren Chen and Cuijuan Li. *A wind tunnel test method on aerodynamic characteristics of moving vehicles under crosswinds*, Journal of Wind Engineering and Industrial Aerodynamics, 2017.

[4] Taro Yamashita, Takafumi Makihara, Kazuhiro Maeda, and Kenji Tadakuma. *Unsteady Aerodynamic Response of a Vehicle by Natural Wind Generator of a Full-Scale Wind Tunnel*, SAE International, 2019.

[5] Wall y+ initial guess, Steve Portal, https://thesteveportal.plm.automation.siemens.com/articles/en_US/FAQ/MP-4-165

[6] Trimmed Mesher, Steve Portal, https://documentation.thesteveportal.plm.automation.siemens.com/starccmplus_latest_en/index.html#page/STARCCMP%2FGUID-DB165A77-56AD-4854-A970-C84BF90B68AD.html%23wwID0EIDX6

[7] Wall y+ based on turbulence model, Steve Portal, https://thesteveportal.plm.automation.siemens.com/articles/en_US/FAQ/EK-5-628

[8] Coupled Flow Solver, Steve Portal, https://documentation.thesteveportal.plm.automation.siemens.com/starccmplus_latest_en/index.html#page/STARCCMP/GUID-50A38509-8CE3-4D06-89AC-6A68BF45626C.html

[9] TECH-SONIC insert datasheet, PSM International, http://www.psminternational.com/en/product/detail.aspx?typeid=1&proid=34

[10] Polymer shrinkage rates, Omnexus, https://omnexus.specialchem.com/polymer-properties/properties/shrinkage#values

[11] Polyhedral mesh, Steve Portal, https://thesteveportal.plm.automation.siemens.com/articles/en_US/FAQ/DS-4-178

[12] Prusa MK3S specifications, PRUSA Research by Josef Prusa, https://www.prusa3d.com/original-prusa-i3-mk3/

A Appendix

A.1 Wind Tunnel Test Template

Wind Tunnel Testing

	Yaw Angle (°)		Yaw Angle (°)	Wind Speed (m/s)	Configuration
Test 1	0	Test 32		Re Sweep	Default
Test 2	0	Test 33	0	25,30,35	Default
Test 3	2.5	Test 34	-2.5	25,30,35	Default
Test 4	5	Test 35	−5	25,30,35	Default
Test 5	7.5	Test 36	-7.5	25,30,35	Default
Test 6	10	Test 37	−10	25,30,35	Default
Test 7	15	Test 38	−15	25,30,35	Default
Test 8	20	Test 39	−20	25,30,35	Default
Test 9	25	Test 40	−30	25,30,35	Default
Test 10	30	Test 41	−40	25,30,35	Default
Test 11	35	Test 42	−50	25,30,35	Default
Test 12	40	Test 43	−60	25,30,35	Default
Test 13	45	Test 44	−70	25,30,35	Default
Test 14	50	Test 45	−80	25,30,35	Default
Test 15	55	Test 46	−90	25,30,35	Default
Test 16	60	Test 47	−100	25,30,35	Default
Test 17	65	Test 48	−110	25,30,35	Default
Test 18	70	Test 49	−120	25,30,35	Default
Test 19	75	Test 50	−130	25,30,35	Default
Test 20	80	Test 51	−140	25,30,35	Default
Test 21	85	Test 52	−150	25,30,35	Default
Test 22	90	Test 53	−160	25,30,35	Default
Test 23	100	Test 54	−170	25,30,35	Default
Test 24	110	Test 55	−180	25,30,35	Default
Test 25	120			25,30,35	Default
Test 26	130			25,30,35	Default
Test 27	140			25,30,35	Default
Test 28	150			25,30,35	Default
Test 29	160			25,30,35	Default
Test 30	170			25,30,35	Default
Test 31	180			25,30,35	Default

A.2 Mounting Plate Drawing

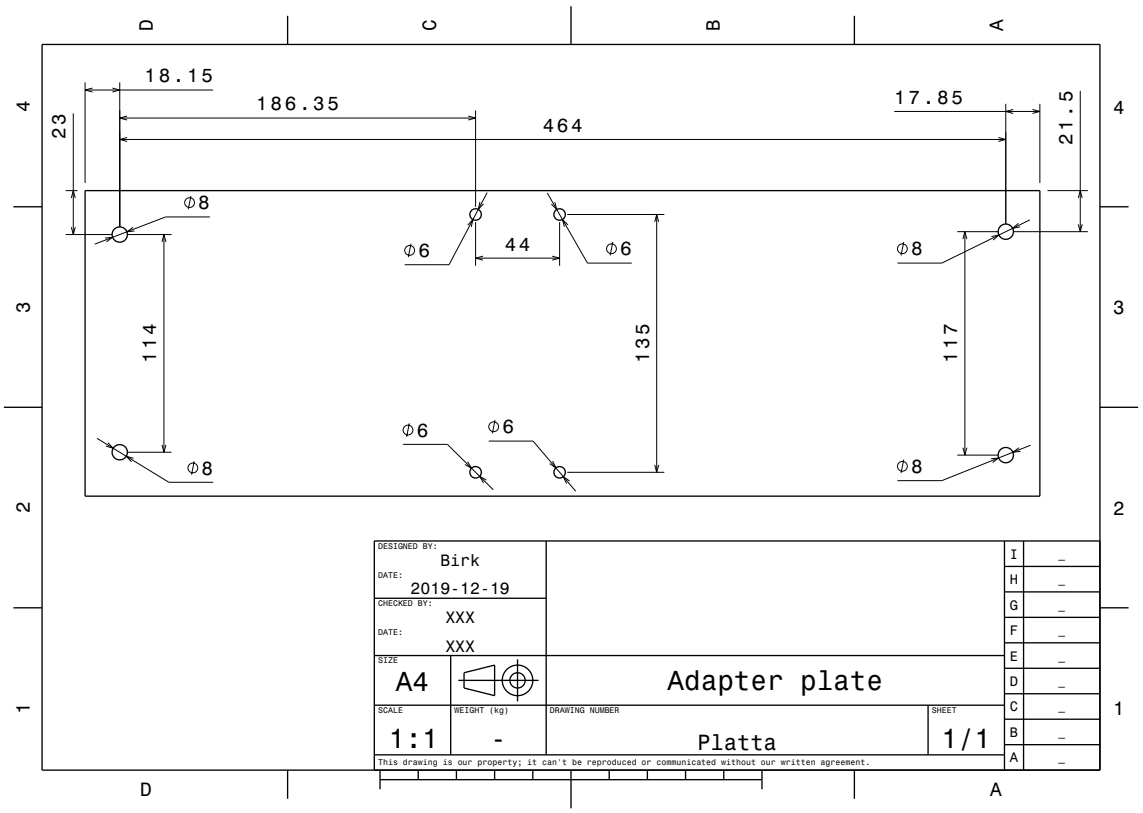

Figure A.1: Drawing of the adapter plate that connects the bus to the scale